UNIVERSITÀ DEGLI STUDI DI PADOVA

DIPARTIMENTO DI FISICA E ASTRONOMIA "G. GALILEI"

Scuola di Dottorato di Ricerca in Fisica
ciclo XXVIII

New approaches to the physics of weakly-bound nuclei: treatment of continuum in ^{6}He

Direttore della scuola:
Chiar.mo Prof. Andrea Vitturi

Supervisore:
Chiar.mo Prof. Lorenzo Fortunato

Dottorando:
Jagjit Singh

A.A. 2015-2016

Contents

List of Figures

List of Tables

"I would like to dedicate this thesis to ***the Almighty, my respected parents & my mentor Dr. Sukhjeet Singh Dhindsa*** *for always guiding me and showing me the right path ... ".*

0.1 Abstract (English)

Nowadays in low energy nuclear physics, the study of properties of the neutron dripline nuclei is a highly interesting topic. The study of the structure of 2n-halo Borromean nuclei demands for a three-body description with proper treatment of continuum, the conventional shell-model assumptions being insufficient. This thesis is focused on the development of a simple nuclear structure model for ground and continuum states of Borromean nuclei. Initially it is tested for ^{6}He, the states of which are built by starting from the continuum single-particle p-states of ^{5}He. The quadrupole response ($0^+ \rightarrow 2^+$) for ^{6}He has been investigated, finding two resonances, the narrow low-lying 2^+ and a broader 2^+ at 2.9 MeV above threshold with a width of about 1.8 MeV. With the aim of studying also negative parity states of ^{6}He, the model space has been extended with inclusion of sd- continuum waves of ^{5}He. The extension of model space is a computationally challenging problem. The role of different continuum components in the weakly bound nucleus ^{6}He is studied by coupling unbound spd-waves of ^{5}He by using simple pairing contact-delta interaction. Our results show that the ^{6}He ground state 0^+ displays collective nature by taking contribution from five different oscillating continuum states i.e. $(s_{1/2})^2$, $(p_{1/2})^2$, $(p_{3/2})^2$, $(d_{3/2})^2$ and $(d_{5/2})^2$, that sum up to give an exponentially decaying bound wavefunction Other ground state properties of ^{6}He have been calculated and compared with other theories and experiments. The two-particle density as a function of the radius $r_1 = r_2 \equiv r$ and the angle θ_{12}, is also calculated, finding two peaks, one at angles smaller than 90^o and one at larger angles, referred to as “di-neutron”and “cigar-like”configurations respectively. Di-neutron component has higher density and it has a longer radial tail, which confirms the halo structure of ^{6}He, while the cigar-like

component has a very compact structure comparatively. We have also investigated electric transitions to the continuum : the monopole(five configurations), dipole (five configurations), quadrupole (seven configurations) and octupole (three configurations) response of the system and contributions of different configurations to these electric multipoles has been discussed. The shapes and total integrated strengths of monopole, dipole and quadrupole response functions are in well agreement with previous studies.

0.2 Sommario (Italiano)

Oggigiorno lo studio delle proprietà dei nuclei vicini alla dripline neutronica è un argomento di grande interesse in fisica nucleare delle basse energie. Lo studio della struttura dei nuclei Borromeani con alone di 2 neutroni richiede una descrizione a tre corpi con un'opportuna trattazione del continuo che il modello a shell tradizionale non fornisce. Questra tesi si concentra sullo sviluppo di un semplice modello di struttura nucleare per lo stato fondamentale e le risonanze nei nuclei Borromeani. Inizialmente viene testata sull'^{6}He, i cui stati sono costruiti a partire da stati p risonanti dell'^{5}He. La risposta per eccitazioni di quadrupolo ($0^+ \rightarrow 2^+$) per l'^{6}He è stata investigata, trovando due risonanze, uno stretto stato 2^+ a bassa energia e uno più largo a 2.9 MeV sopra la soglia con una larghezza di circa 1.8 MeV. In seguito, allo scopo di studiare anche gli stati a parità negativa dell'^{6}He, lo spazio modello è stato esteso con l'inclusione delle onde s e d dell'^{5}He. Il ruolo delle differenti componenti del continuo nel nucleo debolmente legato ^{6}He è stato studiato accoppiando onde *spd* slegate dell'^{5}He per mezzo di una interazione di paring del tipo contact-delta. I risultati mostrano che lo stato fondamentale 0^+ dell'^{6}He mostra una natura collettiva che prende contributi da cinque diversi stati oscillanti del continuo, ovvero $(s_{1/2})^2$, $(p_{1/2})^2$, $(p_{3/2})^2$, $(d_{3/2})^2$ e $(d_{5/2})^2$, che si sommano per dare una funzione d'onda legata che decade con andamento esponenziale. Ulteriori proprietà dello stato fondamentale sono state calcolate e comparate con altre teorie ed esperimenti. Una funzione che rappresenta la densità di due particelle è stata calcolata in funzione del raggio $r_1 = r_2 \equiv r$ e dell'angolo θ_{12}, trovando due picchi, uno ad angoli minori di 90^o e uno ad angoli maggiori, chiamati rispettivamente configurazione a "dineutrone"e a "sigaro". La componente a dineutrone possiede una densità

maggiore e una coda radiale più estesa, che conferma la struttura ad alone dell'^{6}He, mentre la componente a sigaro ha una struttura comparativamente più compatta. Abbiamo anche investigato le transizioni elettriche al continuo: monopolo (5 configurazioni), dipolo (5 configurazioni), quadrupolo (7 configurazioni) e ottupolo (3 configurazioni), discutendo la riposta del sistema e il contributo di ciascuna configurazione. La forma e l'integrale delle funzioni di risposta di monopolo, dipolo e quadrupolo si accordano col risultato di studi precedenti.

0.3 Acknowledgments

I would like to acknowledge the people who supported and otherwise contributed throughout the course of this work.

First of all, I bow with sincere regards to the Almighty for blessing me to accomplish this stalwart work.

I take this opportunity to express my esteem gratitude to ***Dr. Lorenzo Fortunato*** *for his excellent supervision and enormous support in executing this research work. I am indebted to him for fostering the research curiosity and encouragement to engage in the current developments in the field. His exceptional ability to work on different areas of the field always be a motivation for me to lead research as a serious part of my life. I doubt that I will ever be able to convey my appreciation fully, but I owe him with my eternal gratitude.*

I would also like to thank ***Prof. Andrea Vitturi*** *for serving not only as a mentor but also as a co-advisor during the completion of this work. His profound knowledge always captivated me to pursue research with a passion. Certainly, this dissertation would not have been completed without him. I am extremely thankful to the Director* ***Prof. Andrea Vitturi*** *for providing all the research facilities in the institute.*

I also especially thank ***Dr. Rajdeep Chatterjee****, Associate Professor, Department of Physics, Indian Institute of Technology Roorkee, India for his valuable contribution to the research work presented in this thesis and to my general experience during short visit to IITR in summer* 2014.

In support of my work , I bid my special thanks to ***Dr. Sukhjeet Singh Dhindsa*** *who have been blessed with patience to encourage and culminate in the completion of this research. He is more like a mentor in my personal as well as professional growth.*

I am very happy to recall the company of my groupmates ***Dr. José Antonio Lay Valera***, ***Dr. Yasemin Küçük*** , ***Dr. Raj Kumar Gupta*** *and* ***Laura Moschini*** *for fruitful discussions. It is worthy to acknowledge the affection of seniors and love of juniors during this journey.*

This act of devotion and dedication would not have been completed without the moral and emotional support of my respected father ***S. Nirmal Singh Dhindsa*** *and mother* ***Smt Satwant Kaur Dhindsa***. *Special thanks to my uncles* ***S. Mukand Singh Dhindsa***, ***S. Tarsem Singh Dhindsa***, ***Sant Balwinder Singh Bhamri*** *and brother-in -laws* ***S. Jaswant Singh Randhawa***, ***S. Harpal Singh Pawar*** *and* ***S. Navdeep Singh Chahal*** *for their immense help and moral encouragement. I do not know where to begin to thank my other family members and relatives for their sacrifices, love and support. I am extremely grateful to my brother* ***S. Sandeep Singh Dhindsa*** *who worked very hard at different family functions held at my home place during the course of this work. My sincere thanks are for my officemates* ***Giacomo Bighin (UniPD)***, ***Kirill Kanshin (UniPD)*** *and friends* ***Sushil Kumar Rathi(MMU mullana)***, ***Rajeev Bhatia (Ontario, Canada)***, ***Sumit Bhatia (PMB, Qadian, Punjab)***, ***Pardeep Kumar (IITRopar, Punjab)***, ***Baldeep Kaur (TU Patiala)***, ***Gaurav Jayaswal (KAUST)***, ***Varinderdeep Singh (Padova)***, ***William Torres (UniPD)****for their inspiration and solicitous suggestions. I gratefully acknowledge the financial support received from Fondazione Cassa di Risparmio di Padova e Rovigo* ***(CARIPARO)***.

Padova, Italy.

January 2016

Jagjit Singh

Chapter 1

Introduction

1.1 The prelude

Over the past few decades, the nuclei far from the valley of stability, have been one of the main interests for the nuclear physicists. The exploration of new phenomena in unstable nuclei far from the line of stability, has received substantial impulse, due to the recent developments in the radioactive beam facilities around the world [1]. The development of radioactive ion beam (RIB) facilities starts from the early eighties with the pioneer experiment performed at BEVELAC, Berkeley, by Tanihata and his collaborators on ^{11}Li [2, 3]. Since then a large number of RIB facilities has been developed world wide. These include RIBF at RIKEN in Japan [4, 5], FAIR at GSI in Germany [6], FRIB at MSU in the USA [7], SPIRAL2 at GANIL in France [8], ISOLDE in CERN [9], DRIBS at JINR in Dubna [10] and many others which have been, or will soon be, in operation around the world.

With these facilities, high intensity beams of large number of drip line nuclei,

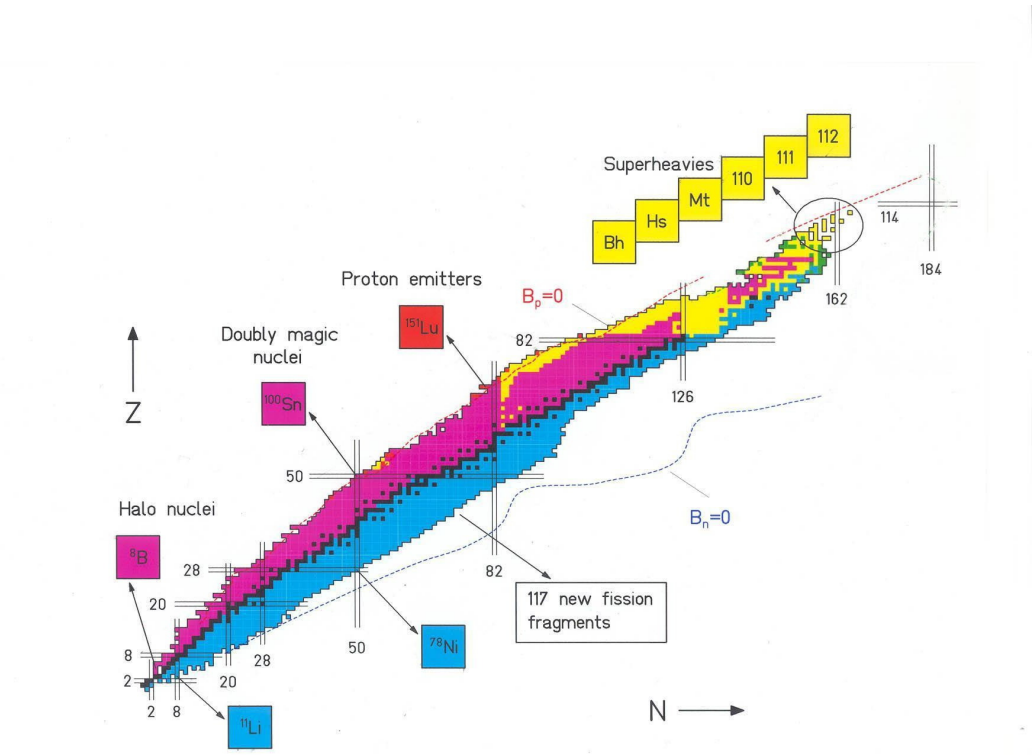

Figure 1.1: The Segré chart of nuclei (adapted from web), the nuclei are organized according to the number of their nucleons, with the neutron number (N) on the horizontal axis and the proton number (Z) on the vertical axis.

which have very short half-lives and very small one- or two-nucleon separation energies of the order of few MeV [11, 12, 13, 14, 15, 16, 17, 18], can be produced and accelerated. This further stimulates the opportunity to boost the existing knowledge of both nuclear structure and reactions at the limits of stability i.e. at driplines (the limit of neutron or proton binding).

In the Fig. (1.1) (also known as the Segré chart), the nuclei are organized according to the number of their nucleons, with the neutron number on the horizontal axis and the proton number on the vertical axis. The few stable nuclei are shown by the black squares. The positions of magic numbers are indicated by horizontal and vertical bars. Above the valley of stability is the proton rich side (shown in magenta) while below it is the neutron rich side

(shown in blue); these are limited by the proton drip line (dashed red) and the neutron drip line (dashed blue), respectively.

At the driplines the binding energy of the last neutron(proton), $B_p(B_n)$, is zero. Due to the hindrance caused to the formation of proton rich nuclei by Coulomb repulsion, the proton drip line is reached quite fast. On the neutron rich side, however, there exist a much larger number of nuclei. In both regions there lie a vast number of nuclei which are yet to be explored. At the extremities of the nuclear chart, nuclear properties are quite different from those encountered in the valley of stability. In the vicinity of driplines, conventional models of nuclear structure encounter severe difficulties in reproducing the large variety of new experimental data such as phenomenon of halo formation at the nuclear surface. Therefore experimental and of course the theoretical studies, in regions away from stability are fields in which there is nowadays an intense research activity.

This chapter is organized as follows. In the next sections 1.2 and 1.3, we will give the definition of halo and Borromean nuclei and discuss their properties. In section 1.4 and 1.5, we will present the motivation for present work along with organization of thesis.

1.2 Halo nuclei

The observation of long tail of matter density distribution in some light drip line nuclei, is linked to the small binding energy of one or two valence nucleons. It was realized that these nuclei, can be described in terms of a core surrounded by a veil of dilute nuclear matter, extending into the classically forbidden region. This veil is what is referred to as "halo"[15, 19, 20] and this special feature was first observed in neutron rich nucleus ^{11}Li [2, 3, 21]. These

halo nuclei are fragile objects. In fact their binding energies are of the order of less than 1 MeV, as compared to the $6-8$ MeV in stable nuclei. There are proton and neutron halos, but the former are rarer and more difficult to produce in laboratory and consequently they have received less attention. We will be interested in the following neutron halos.

The neutron halo is the most interesting phenomena found in some unstable nuclei [2, 19]. Long ago in 1936, immediately after the discovery of neutron, using a beam of neutrons on ^{9}Be target led to the production of first halo nucleus i.e. ^{6}He in the laboratory [22]. Halos were identified in neutron-rich nuclei formed by the neutrons in excess that surrounds the more tightly packed core. There are two main classes of neutron halo states: the two-body halos with one neutron surrounding the core, like the one-neutron halos ^{11}Be [23], ^{14}B [24, 25] and ^{19}C [26] and the three-body neutron halos with two valence neutrons around the core, like two-neutron halos ^{6}He [27], ^{11}Li [2, 3, 28] and ^{14}Be [29, 30].

1.2.1 Features of halo formation

The extreme long tail of the neutron density distribution in these weakly bound nuclei, predicts the tunneling of neutrons outside the core and to be present with appreciable probability at distances much larger than the normal nuclear radius [17]. The root mean square radius of one neutron halo (r^{n}_{rms}) and root mean square $n-n$ separation (r_{nn}) in two neutron halo nuclei are found to be large as compared to the range of nuclear interaction. Qualitatively, one might define a neutron halo state [17, 18] in the coordinate space as the one in which one- or two- neutrons approximately decouple from the remainder of the system and have a large spatial extension, i.e. have more than 50% probability of being outside the binding potential. For a two-body

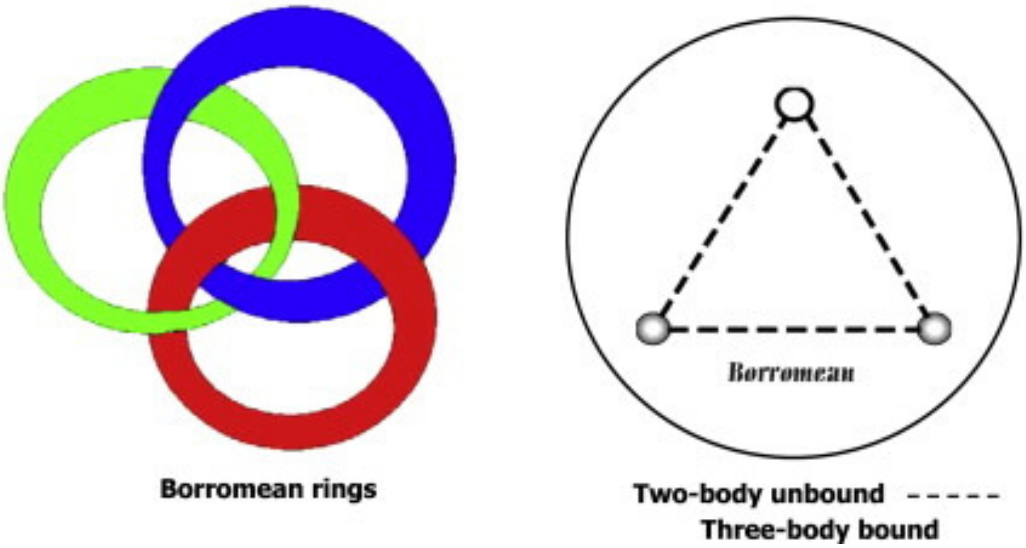

Figure 1.2: The Borromean nucleus consists of a inert core orbited by two neutrons. If any one of the three bodies is removed the remaining two would be unbound, rather like the heraldic Borromean rings. Adapted from Ref [34].

system in s- or p-states the criterion for halo formation is estimated [32, 33] to be

$$E_b < 2A^{-\frac{2}{3}} MeV \tag{1.1}$$

where E_b is the binding energy of the nucleus with mass number A. For example for $A = 6$, the $E_b < 0.6057$ MeV. Some other features of halo structure are the large interaction or reaction cross section, evolution of new magic numbers [39], a narrow momentum distribution [40] and a strong concentration of electric dipole strength at lower excitation energies [41, 42, 43, 44].

1.3 Borromean nuclei

The properties of certain three-body halo nuclei were so intriguing that a new name was coined for them by J.S. Vaagen and M. Zhukov: Borromean

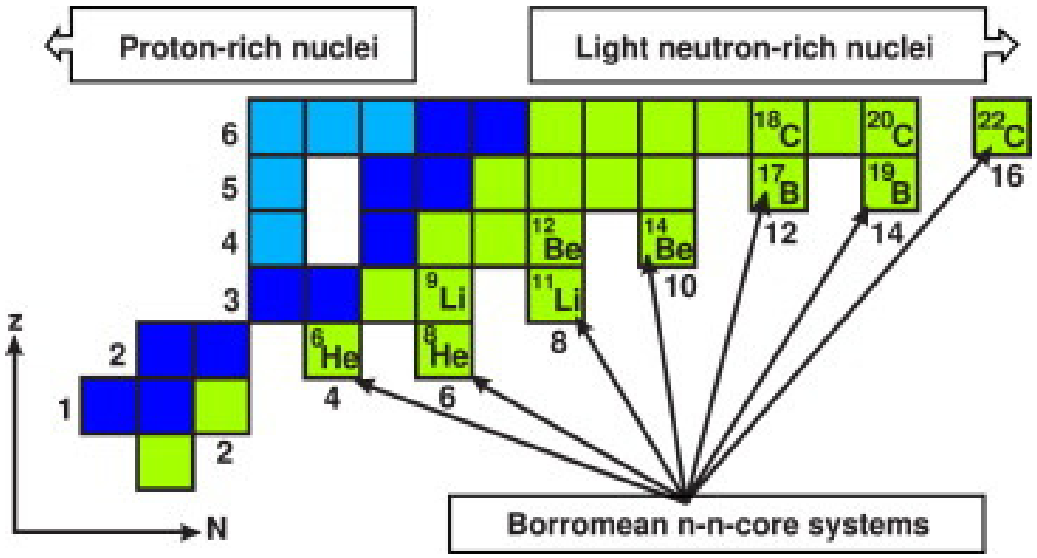

Figure 1.3: Illustrative section of the nuclear chart with isotopes of light halo nuclei with charge number (z) less than 7 and neutron number (N) limited to 16. In particular, we are pointing out the halo-nuclei that, within three-body n−n−core configurations, can be considered as Borromean systems. Adapted from Ref. [35].

nuclei [32]. The name recalls the Borromean rings, heraldic symbol of the princes of Borromeo, which are carved in the stone of their castle on an island in Lake Maggiore in Northern Italy. The three rings are interlocked in such a way that if any of them were removed, the other two would also fall apart as shown in Fig. (1.2). These systems are unique because if any of the three particles is removed, the resulting two-body system is unbound and it falls apart in a very short time. Thus these two-neutron halo nuclei are referred as Borromean nuclei, when there is no bound state between a valence neutron and a core nucleus. Borromean nuclei [32] are many-body nuclear systems that show peculiar features. Borromean nuclei typically have small two-neutron separation energy (S_{2n}). The behavior of Borromean systems is quite different from the standard tightly-bound nuclear systems like ^{42}Ca, or ^{210}Pb, that are far from the drip lines and are only two particles

away from closed shell (A = 40 and A = 208 respectively). In these cases the removal of a single neutron does not alter the system so much as to break it, and subsystems of the (A + n) type, namely ^{41}Ca or ^{209}Pb, are well bound. Usually one can describe the (A + 2n) nuclei by approximating the two-neutron wave function with an appropriate coupling of bound one-particle wave functions. Different is the case of ^{11}Li or ^{6}He, light nuclei close to the neutron drip lines, where the removal of a single neutron makes a big difference because neither ^{10}Li nor ^{5}He exist in bound form. In other words, while the A and (A + 2n) systems are bound, the (A + n) system is unbound. They are usually considered to be made up of three parts: a core that corresponds to a stable bound nucleus plus two weakly bound neutrons (or protons, which is beyond the scope of this thesis). The most studied Borromean nuclei are ^{6}He [27] (system under study), ^{11}Li [2, 3], ^{14}Be [29, 30] and recently observed ^{22}C [36]; their position in the chart of nuclei is shown in Fig. (1.3), together with other two-neutron halo candidates. Notice that there are gap in the chart, ^{5}He, ^{10}Li, ^{13}Be etc. are missing.

1.4 Motivation

On both theoretical and experimental grounds, the two-neutron halo (Borromean) nuclei [70], are yet to be fully understood. The traditional shell model and self-consistent Hartree-Fock calculations, fails to explain the properties of these nuclei, because of the scattering of nucleons from bound states to unbound continuum states. In study of these systems, continuum plays a vital role and it demands proper treatment. With the motivation of treatment of continuum as an important issue, we have developed of a simple theoretical structure model for ground and continuum states of Borromean

nuclei. Initially it is tested for ^{6}He [82, 97, 98, 99] to study the weakly bound ground state and low-lying continuum states of ^{6}He by coupling two unbound spd-waves of ^{5}He. In our approach, rather than simulating the resonance with a bound wave function, we calculate the full continuum single-particle spectrum of ^{5}He in a straightforward fashion and use two copies of the oscillating continuum wave functions to construct two-particle states. These states must necessarily have a positive defined energy for each type of relative motion angular momentum. One must resort to the binding effect of some residual interaction, in our case a simple pairing interaction (favoring the lowest angular momenta), to bring one of the many unbound energy eigenvalues down into the bound regime following Ref. [91, 92] for the L= 0 case. The main aim of this thesis is to show how an extension of the calculations of the effects of the residual interactions from coupled bound states to coupled continuum states naturally explains the stable character of the bound states of Borromean nuclei, such as ^{6}He, and simultaneously accounts for some of the resonant structures seen in the low-lying energy continuum. The diagonal and nondiagonal matrix elements of the residual interaction give a nontrivial contribution that furnishes an utterly convincing explanation for the level structure of these nuclei.

1.5 Outline of the thesis

Thesis is divided into six chapters. After the introduction, we discuss brief experimental and theoretical investigations on ^{6}He (chapter 2) followed by the model formulation and procedure adopted is presented in chapter 3 and appendix A respectively. In chapter 4 we investigate the intermediate unbound system ^{5}He, in simple fashion. In chapter 5 we set up of basic ingredients

needed for the calculations is presented along with some results on ground state properties of ^{6}He. Finally in chapter 6 we discuss the electromagnetic response of the ^{6}He, followed by conclusions and future perspectives. The formulation, procedure and various results discussed in thesis have been already published in three articles [82, 97, 98] and while the results using the extended model space are germaine to this work and their publication will soon follow the completion of the present thesis. [99].

Chapter 2

Experimental and theoretical investigations on ^{6}He

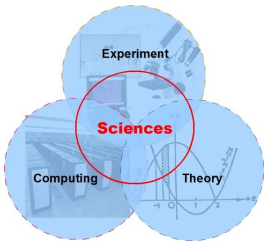

2.1 Initial remarks

The vast sea of theoretical and experimental work on the two-neutron halo (Borromean) nuclei, raises the attention of nuclear physics community for these systems. In this chapter we will present some of the experimental observations and proposed theoretical models, focused on the results obtained for ^{6}He.

This chapter is organized as follows. In the section 2.2, we will present the detailed chronological order of experimental literature survey. In the section 2.3, we will discuss the various theories focused on results for ^{6}He and finally we will draw some conclusions.

2.2 Experimental spectroscopy of ^{6}He

Due to diminishing half-lives and narrow production cross sections, the experimental analysis of these dripline systems is a challenging issue. In these weakly-bound nuclear systems, the properties of the continuum states become progressively more and more fundamental to the nuclear structure and reactions. A low breakup threshold introduces many new features such as large spatial density distribution [2, 3], evolution of new magic numbers [39], a narrow momentum distribution [40] and a strong concentration of electric dipole strength at lower excitation energies [41, 42, 43, 44] in these systems. ^{6}He is a well established two neutron halo nucleus. Experimentally the higher excited states of ^{6}He are still under discussion and are not very clear.

In the eighties the $J^\pi = 0^+$ ground state and first excited $J^\pi = 2^+$ state at energy 1.797 MeV have been confirmed in numerous reactions [46, 47]. However, (n,p) spectra measured at a lower bombarding energy of 60 MeV [46] and summed over the angular range from 6.5° to 32.5° display additional broad structures at energies 15.5 MeV (Γ = 4 MeV) and 25 MeV (Γ = 8 MeV), where Γ is the width of structures. However, inconsistencies have been reported [47] including the possible splitting of the 15.5 MeV resonance into two or three components over the range of energy $13-18$ MeV, as observed in the reactions ^{7}Li(p,2p)^{6}He [49], ^{7}Li(n, d)^{6}He [50], ^{6}Li(e$^-$, π^+)^{6}He, and ^{6}Li(γ, π^+)^{6}He [51]. All of the reported levels of which we have found information for E $\leq$ 25 MeV are included in Fig. (2.1).

In late nineties, the ^{6}Li(^{7}Li, ^{7}Be)^{6}He charge-exchange reaction has been studied at E(^{7}Li) = 350 MeV and transitions to the known $J_\pi = 0^+$ ground state and the $J_\pi = 2^+$ state at E_x = 0.0 and 1.8 MeV (weak) and three strong and broad resonances at $E_x \approx 5.6, 14.6$ and 23.3 MeV have been

observed [52]. Also the strong resonances at ~ 5.6 MeV and ~ 14.6 MeV are interpreted as 2^+ and $(1,2)^-$ resonances, respectively.

In early 21st century, a dipole excitation concentrated at low-excitation energies (E $= 4 \pm 1$ MeV and $\Gamma = 4 \pm 1$ MeV) was observed via the ^{6}Li(^{7}Li, ^{7}Be) reaction at 65A MeV [53, 54].

In charge exchange reactions between two fast colliding nuclei ^{6}Li(t, ^{3}He)^{6}He reaction at 336 MeV, a broad asymmetric structure at energy ~ 5 MeV and another structure at 14.6 MeV above the strong peaks for the ground and first excited states in ^{6}He have been observed [55, 56]. The angular distributions show that the structure around 5 MeV is dominated by the dipole states with a mixture of positive parity states in its lower-energy portion. Different mechanisms have also been proposed to explain this mode and this phenomenon is still under debate.

In the same year Akimune et al., observed resonances above the t + t threshold in ^{6}He via the ^{6}Li(^{7}Li, ^{7}Be t)^{3}H reaction with a ^{7}Li beam of 65 MeV/nucleon [57]. A new prominent resonance was found at energy 18.0$\pm$0.5 MeV with a width of 7.7 ± 1.0 MeV.

More recently, with the two-neutron transfer reaction p(^{8}He,t) at the SPIRAL facility at 15.4 AMeV (GANIL, Caen), a much narrower 2^+ ($\Gamma = 1.6$ MeV) state and a $J = 1$ resonance ($\Gamma \sim 2$ MeV) of unassigned parity at energies 2.6 and 5.3 MeV respectively have been populated [58].

It is worthwhile to mention that a very new reaction ^{3}H(α,$p\alpha$)$2n$ with a four-body exit channel, induced by the interaction of alpha-particles at energy of $E_\alpha = 67.2$ MeV, apparently shows the existence of ten resonant states [59]. The most part of these states are narrow resonances, as their total width is less than the energy of a resonance. Fig. (2.1) presents the chronological order of experimental data on ^{6}He. As it appears from this

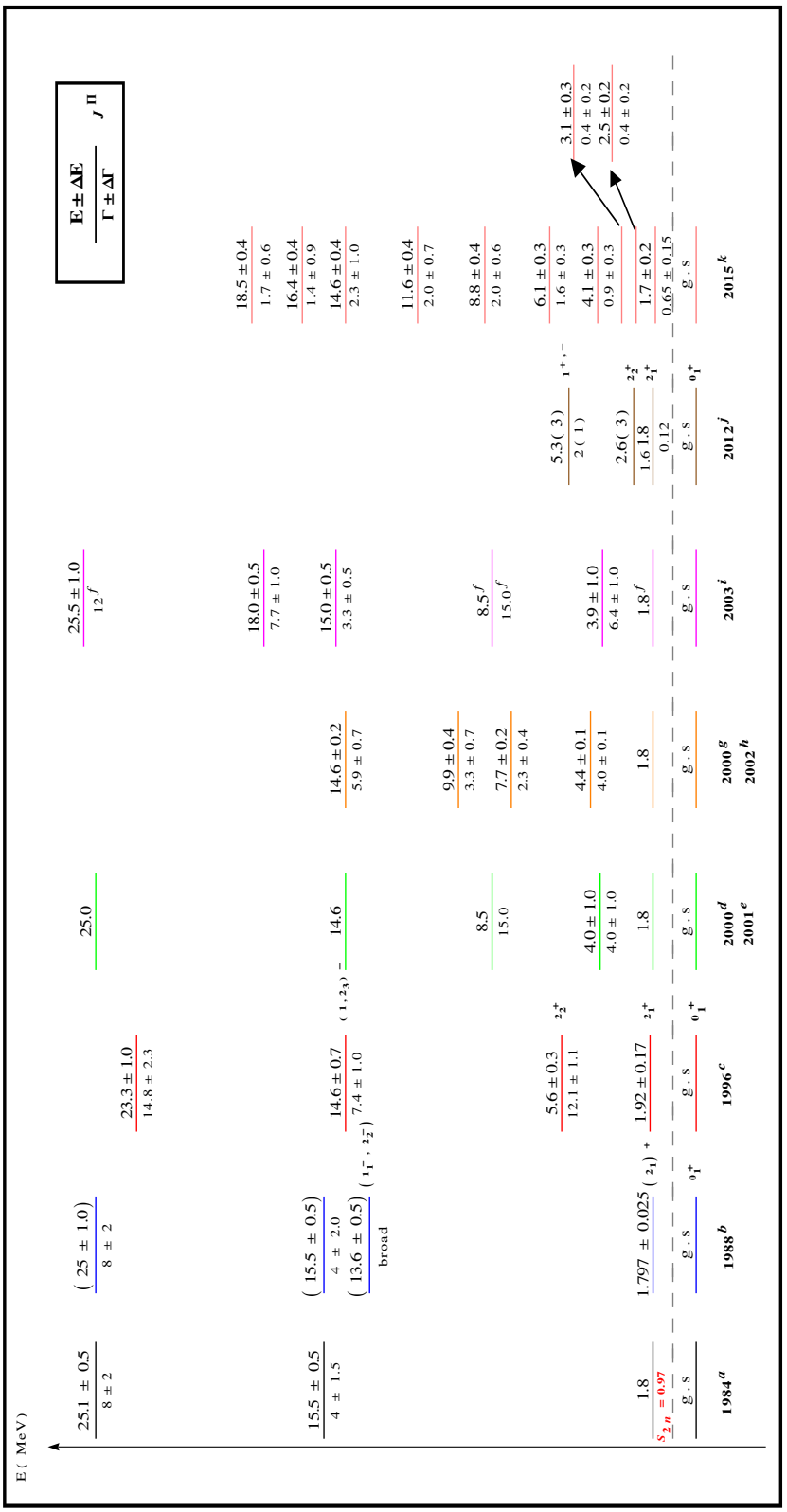

Figure 2.1: Summary of the experimental spectroscopy of ^{6}He at the time of writing. [a]Reference [46], *(n,p)* at 60 MeV/nucleon. [b]Reference [47]. [c]Reference [52], (^{7}Li, ^{7}Be) at 50 MeV/nucleon. [d,e]Reference [53, 54], (^{7}Li, ^{7}Be) at 65 MeV/nucleon. [g,h]Reference [55, 56], (t, ^{3}He) at 112 MeV/nucleon. [i]Reference [57], (^{7}Li, ^{7}Be t) at 65 MeV/nucleon. [j]Reference [58], (^{8}He, t) at 15.4 MeV/nucleon. [k]Reference [59], (α, $p\alpha$) at 67.2 MeV/nucleon. [f]Fixed in fits.

picture, there is no general consensus on the spectrum and the role of the continuum is far from being understood. Our effort to try and clarify this picture from a theoretical point of view, stems from general considerations enumerated here.

2.3 Theoretical Investigations on ^{6}He

On the theoretical side the the treatment of low breakup thresholds, responsible for strong coupling of bound and continuum states is the challenging issue. Theoretically, the 2n-halo structure of ^{6}He was investigated, the many predictions, all incomplete in different ways, suggest a sequence of levels 0^+_{gs}, 2^+_1, 2^+_2, 1^+, 0^+_1, but disagrees on their positions and widths.

In early seventies, Migdal [60] gave a qualitative argument in order to explain the stability of systems made of a core, A, plus two neutrons despite the intermediate system (A + n) being unbound. He linked the presence of a resonant state in the continuum of the intermediate system to the stability of (A + 2n) system. The whole continuum in this approach is approximated with a single resonant state to which global averaged properties are attributed, discarding the specificity of the continuous spectrum.

Later in late eighties Hansen and Jonson [19] proposed that many of the properties of two-neutron Borromean systems can be studied and explained within a two-body model that describes the system with a core plus a dineutron cluster. It is clearly a coarse, but well-working, approximation for a correlated pair of neutrons, that interact via a nucleon-nucleon potential. The dineutron is an idealization that would not exist alone in a bound form, but can be thought of existing in medium due to the stabilizing or binding presence of the core′s mean field.

In simple shell model picture of ^{6}He two neutrons outside the alpha particle core, sits in p-shell. Most of the ^{6}He structure predictions took only p-shell excitations into account, but more complete picture must include the promotion of neutrons to $sd-$shell. In particular $sd-$shell plays a vital role, allowing the possibility of dipole excitations to the continuum. The halo structure of ^{6}He is quite well understood by ^{4}He$+n+n$ model. The binding energy is underestimated by a small amount (~ 0.2 MeV) than the observed value and this suggests that ^{4}He core excitations might be important, which are not taken into account [61, 62, 63].

In order to understand the weak binding characteristics of light nuclei close to drip line, the continuum coupling effects have been investigated with in various frameworks, the Gamow Shell model [64, 65, 66, 67], the Continuum Shell Model [68], the Complex Scaled Cluster Orbital Shell Model [69] and the Hyperspherical Harmonics Expansion [70]. All these nuclear models are successful in predicting the ground state and first excited state structure to a reasonable degree, but they disagree for predictions of other higher excited states.

The Quantum Monte Carlo p-shell calculations [71], along with well established ground state and first excited state structure, predicts the energy of the excited 0^+ state at about 4.66 MeV, depending on the interaction used. In other calculations, the energy of the excited 0^+ state might be as low as 4.9 MeV [69] or as high as 8 MeV [66]. The energy of the 1^+ state covers the range of 3.4 [66] to 8 [72] MeV.

On the other hand, in few-body calculations [74], the two 0^+ states were nearly pure jj-coupled states. This calculation allowed excitations into the sd-shell, but these turned out to be small for the g.s. and even less for the excited 0^+ state. The sd-shell occupancy was larger for the 2^+ states.

Recently the 0^+ ground state (g.s.) of ^{5}He has been calculated by using bound, exponentially decaying, single-particle shell model states for the sake of simplicity [75]. While this is an insightful assumption that allows several conclusions to be drawn, because of the fact that the (A+n) system is unbound, a more general treatment can be proposed that accounts simultaneously for the bound and continuum states of both the (A+n) and the (A+2n) systems. A standard procedure consists in approximating the one-particle resonance or continuum state (E$>$ 0) with a bound state (E$<$ 0) with appropriate quantum numbers and then construct two-particle states. The unperturbed two-particle energy is then shifted by the matrix elements of a suitable pairing interaction, most often a contact delta interaction or a Gaussian potential.

In order to avoid the uncertainties due to the the treatment of α particle as point particle, recently reference [76] study the ^{6}He nucleus in a fully microscopic six-nucleon calculations. Results claim that the E1 strength function exhibits a two-peak structure at around 3 and 33 MeV excitation energy. The lower peak is well understood in the framework of the α+n+n structure and its excitation mechanism is consistent with the classical interpretation of the soft dipole mode (SDM). The higher peak is the typical giant dipole resonance that exhibits out-of-phase proton-neutron collective oscillations. Just a few MeV above the SDM peak, some new modes are found that can be regarded as a vibrational excitation of the SDM.

Among the phenomenological models, the work of Esbensen et al. [85] deserves a particular mention, as it discusses the merits and limitations of the no-recoil approximation. The paper shows that some observables take different values depending on the inclusion or exclusion of recoil effects, but in general it concludes that the no-recoil approximation works quite well.

The proper inclusion of these effects becomes necessary when dealing with dipole strength, as in Ref. [77].

All these theoretical frameworks have been used to describe the ground state structure to a reasonable degree and to approximate the dynamics of nuclear reactions fairly well, but for the most part they still do not incorporate effects due to the presence of the continuum. These are essential to understand the prime reason of the stable character of ^{6}He. Only very recently in Ref. [78] the continuum has been included, they found several resonances, including the well-known narrow 2^+_1 and the recently measured broader 2^+_2. Additional resonant states emerged in the $2^-$and 1^+ channels near the second 2^+ resonance and in the 0^- channel at slightly higher energy.

2.4 Conclusions

With all these detailed theoretical and experimental review, we are highly motivated to implement the recently developed simple theoretical structure model, to study the ground and continuum states properties for ^{6}He [82, 97, 98, 99], by coupling two unbound spd-waves of ^{5}He.

Chapter 3

Formulation and procedure

3.1 Initial remarks

The two-neutron halo (Borromean) nuclei [70] are not yet fully understood and are still able to attract the attention of nuclear physics community. For these systems, the traditional shell-model picture is inappropriate, because of the scattering of nucleons from bound states to unbound continuum states. The phenomenological models [85, 86, 87] and *ab initio* models [72, 73, 88, 89, 71] are successful in describing their structure to a reasonable degree and to approximate their behavior in nuclear reactions fairly well, but they still fail to incorporate effects due to the presence of the continuum. These are essential to understand the prime reason of their stable character. In fact these approaches normally take as a starting point for calculations not the true continuum, but rather a basis set of bound, exponentially decaying wave functions (obtained, for example, from a diagonalization in a box of finite radius). The key idea of this work is to show how an extension of the

calculations of the effects of the residual interactions from coupled bound states to coupled continuum states naturally explains the stable character of the bound states of Borromean nuclei, such as ^{6}He, and simultaneously accounts for some of the resonant structures seen in the low-lying energy continuum. The paradigm for this approach is taken from the successful calculation of properties of deeply-bound nuclei that have two particles outside of a doubly magic core: for example see the discussion in Heyde´s textbook [93] on ^{18}O, a deeply bound nucleus where the continuum does not play any role. The diagonal and non-diagonal matrix elements of the residual interaction give a nontrivial contribution that furnishes an utterly convincing explanation for the level structure of these nuclei. Based on this description of standard nuclear systems having two-particles outside closed shells, there have been several studies [91, 92] aimed at showing how Borromean systems are bound due to the effect of pairing that brings the energy of the subsystem below the neutron emission threshold. The short-range nature of the residual NN interaction between the otherwise unbound neutrons is what kills the oscillating tail of the continuum wave functions. Motivated by the recent experimental measurements at GANIL [58, 59], on continuum resonances in ^{6}He, we have developed a simple theoretical model [82, 97, 98, 99] to study the weakly bound ground state and low-lying continuum states of ^{6}He by coupling five unbound spd-waves of ^{5}He. In our approach, rather than simulating the resonance with a bound wave function, we calculate the full continuum single-particle spectrum of ^{5}He in a straightforward fashion and use two copies of the oscillating continuum wave functions to construct two-particle states. The simple pairing contact-delta interaction is used and pairing strength is adjusted to reproduce the bound ground state of ^{6}He. Initially it is tested for ^{6}He, starting from the continuum single-particle p-states

of ^{5}He. Quadrupole response ($0^+ \rightarrow 2^+$) for ^{6}He has also been investigated, finding two resonances, the narrow low-lying 2^+ and a broader 2^+ at 2.9 MeV above threshold with a width of about 1.8 MeV [82]. In order to complete the study, I had extended model space by including sd- continuum states which is a quite computationally challenging [97, 98, 99]. The extension of model space will also allow me to calculate the monopole, dipole response of the system and to disentangle the ambiguous nature of the $1^{(-)}$state recently measured [58]. This simple model accounts for the stable character of the bound states of Borromean nuclei in a natural way, such as ^{6}He and simultaneously accounts for some of the resonant structures seen in the low-lying energy continuum. This chapter is organized as follows. In the next sections 3.2 to 3.4, we will discuss the theoretical formalism used for the crudest model with two non-interacting particles in the single-particle levels of ^{5}He. In appendix A we recall the outline of the procedure that allows the calculation of different configurations of ^{6}He including continuum states and we set up basic ingredients for computations.

3.2 Two-particle wave functions

The two-particle wave functions are constructed by tensor coupling of two continuum states of ^{5}He. Each single particle continuum wavefunction, as a function of radial variable and continuum energy, is given by

$$\phi_{\ell,j,m}(\vec{r}, E_C) = \phi_{\ell,j}(r, E_C)[Y_{\ell m_\ell}(\Omega) \times \chi_{1/2,m_s}]^{(j)}_m \tag{3.1}$$

The combined tensor product of these two single-particle continuum wavefunctions is given by

$$\psi_{JM}(\vec{r}_1,\vec{r}_2) = [\phi_{\ell_1,j_1,m_1}(\vec{r}_1,E_{C1}) \times \phi_{\ell_2,j_2,m_2}(\vec{r}_2,E_{C2})]^{(J)}_M \tag{3.2}$$

The two-particle wave functions in $LS-$ and $jj-$ couplings are connected through the following relation [100] :

$$\begin{aligned}\psi\left(\ell_1 j_1 \ell_2 j_2 JM\right) = \quad & \sum_{S,L} \sqrt{(2S+1)(2L+1)(2j_1+1)(2j_2+1)} \\ & \begin{Bmatrix} 1/2 & \ell_1 & j_1 \\ 1/2 & \ell_2 & j_2 \\ S & L & J \end{Bmatrix} \psi\left(\ell_1 \ell_2 SLJM\right)\end{aligned} \tag{3.3}$$

In LS-coupling for $\ell_1 \neq \ell_2$ the antisymmetric wavefunction $\psi\left(\ell_1\ell_2SLJM\right)$ is given by [100]

$$\begin{aligned}\psi\left(\ell_1\ell_2SLJM\right) = \frac{1}{\sqrt{2}} \sum_{M_S,M_L} \langle SM_SLM_L|SLJM\rangle \times \\ [\phi_{12}(\ell_1\ell_2LM_L)\chi_{12}(s_1s_2SM_S) - \phi_{21}(\ell_2\ell_1LM_L)\chi_{21}(s_2s_1SM_S)]\end{aligned} \tag{3.4}$$

By making use of symmetry relations, Eq.(5.3) can be written as

$$\begin{aligned}\psi\left(\ell_1\ell_2SLJM\right) = \frac{1}{\sqrt{2}} \sum_{M_S,M_L} \langle SM_SLM_L|SLJM\rangle \times \\ [\phi(\ell_1\ell_2LM_L) + (-1)^{(\ell_1+\ell_2-L+S)}\phi(\ell_2\ell_1LM_L)]\chi(s_1s_2SM_S)\end{aligned} \tag{3.5}$$

Here $\phi(\ell_2\ell_1LM_L)$ is the wavefunction for particle 1 in ℓ_2-orbit and particle 2 in ℓ_1 -orbit and ℓ_2 and ℓ_1 are coupled to the same final L. The other

ingredients are defined as follows:

$$\phi(\ell_1\ell_2 LM_L) = \sum_{m_1 m_2} \langle l_1 m_1 l_2 m_2 | l_1 l_2 L M_L \rangle \phi_1(l_1 m_1)\phi_2(l_2 m_2) \tag{3.6}$$

$$\phi(\ell_2\ell_1 LM_L) = \sum_{m_1 m_2} \langle l_2 m_2 l_1 m_1 | l_2 l_1 L M_L \rangle \phi_1(l_2 m_2)\phi_2(l_1 m_1) \tag{3.7}$$

$$\chi(s_1 s_2 S M_S) = \sum_{m_s m_s'} \left\langle \frac{1}{2} m_s \frac{1}{2} m_s' \middle| \frac{1}{2}\frac{1}{2} S M_S \right\rangle \chi_1(m_s)\chi_2(m_s') \tag{3.8}$$

So we have rewritten an antisymmetrized wavefunction by a linear combination of different functions in which particles appear in a given order.

3.3 Matrix elements of interaction

The matrix elements due to mutual interaction V_{12} of two particles are given in LS-coupling by

$$\Delta E_J = \int \psi^* \left(\ell_1\ell_2 SLJM\right) V_{12} \psi \left(\ell_1\ell_2 SLJM\right) \tag{3.9}$$

Substituting twice Eq.(3.5) in Eq.(3.9) we arrive at

$$\begin{aligned} \Delta E_{SLJ} \quad &= \frac{1}{2}\{\langle \ell_1\ell_2 SLJM | V_{12} | \ell_1\ell_2 SLJM\rangle + \langle \ell_2\ell_1 SLJM | V_{12} | \ell_2\ell_1 SLJM\rangle \\ &+(-1)^{(\ell_1+\ell_2-L+S)}[\langle \ell_1\ell_2 SLJM | V_{12} | \ell_2\ell_1 SLJM\rangle \\ &+\langle \ell_2\ell_1 SLJM | V_{12} | \ell_1\ell_2 SLJM\rangle]\} \end{aligned} \tag{3.10}$$

Using the following symmetries

$$\langle \ell_1\ell_2 SLJM | V_{12} | \ell_1\ell_2 SLJM\rangle = \langle \ell_2\ell_1 SLJM | V_{12} | \ell_2\ell_1 SLJM\rangle \tag{3.11}$$

and

$$\langle \ell_1 \ell_2 SLJM|V_{12}|\ell_2 \ell_1 SLJM\rangle = \langle \ell_2 \ell_1 SLJM|V_{12}|\ell_1 \ell_2 SLJM\rangle \qquad (3.12)$$

from Eqs.(3.10), (3.11) and (3.12) we get

$$\begin{aligned} \Delta E_{SLJ} &= \langle \ell_1 \ell_2 SLJM|V_{12}|\ell_1 \ell_2 SLJM\rangle + \\ & (-1)^{(\ell_1+\ell_2-L+S)} \langle \ell_1 \ell_2 SLJM|V_{12}|\ell_2 \ell_1 SLJM\rangle \end{aligned} \qquad (3.13)$$

By following similar considerations the matrix elements due to mutual interaction V_{12} in jj-coupling of two particles for $j_1 \neq j_2$ are given by

$$\begin{aligned} \Delta E_{j_1 j_2 J} &= \langle \ell_1 j_1 \ell_2 j_2 JM|V_{12}|\ell_1 j_1 \ell_2 j_2 JM\rangle + \\ & (-1)^{(j_1+j_2-J)} \langle \ell_1 j_1 \ell_2 j_2 JM|V_{12}|\ell_2 j_2 \ell_1 j_1 JM\rangle \end{aligned} \qquad (3.14)$$

It should be noted that the matrix elements in Eq.(3.13) have the usual meaning i.e.

$$\begin{aligned} &\langle \ell_a \ell_b SLJM|V_{12}|\ell_c \ell_d S'L'J'M'\rangle = \\ &\sum \langle SM_S LM_L|SLJM\rangle \langle S'M'_S L'M'_L|S'L'J'M'\rangle \\ &\langle s_1 m_{s_1} s_2 m_{s_2}|s_1 s_2 SM_S\rangle \langle s'_1 m'_{s_1} s'_2 m'_{s_2}|s'_1 s'_2 S'M'_S\rangle \\ &\langle \ell_a m_a \ell_b m_b|\ell_a \ell_b LM_L\rangle \langle \ell_c m_c \ell_d m_d|\ell_c \ell_d L'M'_L\rangle \\ &\int [\phi_1(a)\chi_1(m_{s_1})\phi_2(b)\chi_2(m_{s_2})]^* V_{12} [\phi_1(c)\chi_1(m'_{s_1})\phi_2(d)\chi_2(m'_{s_2})] d\vec{r}_1 d\vec{r}_2 \end{aligned} \qquad (3.15)$$

where quantum numbers ℓ_a and ℓ_c are associated with particle 1, ℓ_b and ℓ_d are associated with particle 2. ℓ_a and ℓ_b are coupled to L and ℓ_c and ℓ_d are coupled to L'. Thus the matrix elements of interaction i.e. Eq.(3.13) contains two terms: the *direct term* $\langle \ell_1 \ell_2 SLJM|V_{12}|\ell_1 \ell_2 SLJM\rangle$ and the *ex-*

change term $\langle \ell_1 \ell_2 SLJM | V_{12} | \ell_2 \ell_1 SLJM \rangle$. If ℓ_1 is different from ℓ_2 i.e. their overlap in space is very small, the contribution of exchange term will become very small. For completely non-overlapping orbits the contribution of the exchange term vanishes and we are left with the direct term. Only for considerably overlapping orbits, the exchange terms plays a significant role. From Eq.(3.13) one may wonder that for spin-independent interactions the contribution of exchange terms has different signs for states with $S = 0$ and $S = 1$. This is due to the fact that spin-dependent part of the wave function is symmetric for $S = 0$ with respect to exchange of coordinates and antisymmetric for $S = 1$ in the space coordinates [100]. By separating radial and angular dependence of $\phi(n\ell m)$ as

$$\phi(n\ell m) = u_{n\ell}(r)\, Y_{\ell m}(\Omega) \tag{3.16}$$

where $u_{n\ell}(r) = \frac{R_{n\ell}(r)}{r}$ and $\Omega = (\theta, \varphi)$, and with proper choice of pairing interaction V_{12}, Eq.(3.15) can be simplified as in following section.

3.4 Pairing Interaction

Since last five decades the effective density-dependent interactions have been used to study the pairing phenomena [101]. The standard way to simulate the neutron-neutron interaction is the use of density dependent delta interaction. In $(T = 1, S = 0)$ channel, the interaction between two neutrons has strong attraction and is approximated by a contact interaction. The effective interaction V_{nn} between the valence neutrons is given by

$$V_{nn}(\vec{r}_1 - \vec{r}_2) = \delta(\vec{r}_1 - \vec{r}_2) \left(\upsilon_0 + \frac{\upsilon_\rho}{1 + exp[(r_1 - R_\rho)/a_\rho}} \right) \tag{3.17}$$

The first term in Eq.(3.17) is the density-independent part of the interaction and is characterized by one parameter namely its strength. The second term in Eq.(3.17) is the density-dependent part of the interaction and is characterized by three parameters. The spatial symmetry effects of the wave function can be studied by careful choice for V_{12}. We prefer to choose a simpler interaction rather then implementing a density dependent interaction that would need more geometric parameters depending on the particular functional form of the interaction. We take an attractive pairing contact delta interaction. With simple attractive pairing contact delta interaction we can reach the goal of calculation of monopole, dipole, quadrupole and octupole response with only four parameters (the pairing strengths in the $J = 0, 1, 2$ and 3 channels). For $S = 0$, i.e. spin independent case, the explicit expression for V_{12} is given by

$$V_{12} = -g\delta\left(r_1 - r_2\right) \tag{3.18}$$

where

$$\delta\left(r_1 - r_2\right) = \frac{1}{r_1 r_2}\delta\left(r_1 - r_2\right)\delta\left(cos\theta_1 - cos\theta_2\right)\delta\left(\varphi_1 - \varphi_2\right) \tag{3.19}$$

For the moment we drop the index J of the pairing strength g, but in the next chapters we will elaborate on this dependence. Using Eq.(3.16) and Eq.(5.5) and making use of the fact that V_{12} is spin independent, the integral in Eq.(3.15) can be rewritten as

$$\begin{aligned}\int [\phi_1(a)\chi_1(m_{s_1})\phi_2(b)\chi_2(m_{s_2})]^* V_{12}[\phi_1(c)\chi_1(m'_{s_1})\phi_2(d)\chi_2(m'_{s_2})]d\vec{r}_1 d\vec{r}_2 \\ = \int R^*_{n_a\ell_a}(r)\, R^*_{n_b\ell_b}(r)\, \frac{1}{r^2} R_{n_c\ell_c}(r)\, R_{n_d\ell_d}(r)\, dr \\ \int Y^*_{\ell_a m_a}(\Omega)\, Y^*_{\ell_b m_b}(\Omega)\, Y_{\ell_c m_c}(\Omega)\, Y_{\ell_d m_d}(\Omega)\, d\Omega \end{aligned} \tag{3.20}$$

For all the formulation we have used the conventions followed by Talmi [100]. Using the property of two spherical harmonics of same angles

$$[Y_{\ell_a m_a}(\Omega)\, Y_{\ell_b m_b}(\Omega)]^* = \sum_{\ell,m} (-1)^{\ell-m} \begin{pmatrix} \ell & \ell_a & \ell_b \\ -m & m_a & m_b \end{pmatrix} \langle \ell \| Y_{\ell_a} \| \ell_b \rangle^* Y_{\ell m}(\Omega)^*$$

$$[Y_{\ell_c m_c}(\Omega)\, Y_{\ell_d m_d}(\Omega)] = \sum_{\ell',m'} (-1)^{\ell'-m'} \begin{pmatrix} \ell' & \ell_c & \ell_d \\ -m' & m_c & m_d \end{pmatrix} \langle \ell' \| Y_{\ell_c} \| \ell_d \rangle Y_{\ell' m'}(\Omega) \tag{3.21}$$

together with the orthonormal property of spherical harmonics i.e.

$$\int Y^*_{\ell m} Y_{\ell' m'} d\Omega = \delta_{\ell\ell'} \delta_{mm'} \tag{3.22}$$

we are left with

$$\int Y^*_{\ell_a m_a}(\Omega)\, Y^*_{\ell_b m_b}(\Omega)\, Y_{\ell_c m_c}(\Omega)\, Y_{\ell_d m_d}(\Omega)\, d\Omega = \sum_{\ell,m} (-1)^{2(\ell-m)} \begin{pmatrix} \ell & \ell_a & \ell_b \\ -m & m_a & m_b \end{pmatrix} \begin{pmatrix} \ell & \ell_c & \ell_d \\ -m & m_c & m_d \end{pmatrix} \langle \ell \| Y_{\ell_a} \| \ell_b \rangle^* \langle \ell' \| Y_{\ell_c} \| \ell_d \rangle \tag{3.23}$$

Hence using above assumptions and properties Eq.(3.15) is reduced to

$$\begin{aligned}
&\langle \ell_a \ell_b SLJM|V_{12}|\ell_c \ell_d S'L'J'M'\rangle = \\
&g\sum \langle SM_S LM_L|SLJM\rangle \langle S'M'_S L'M'_L|S'L'J'M'\rangle \\
&\langle s_1 m_{s_1} s_2 m_{s_2}|s_1 s_2 SM_S\rangle \langle s'_1 m'_{s_1} s'_2 m'_{s_2}|s'_1 s'_2 S'M'_S\rangle \\
&\langle \ell_a m_a \ell_b m_b|\ell_a \ell_b LM_L\rangle \langle \ell_c m_c \ell_d m_d|\ell_c \ell_d L'M'_L\rangle \\
&\sum_{\ell m}(-1)^{2(\ell-m)} \begin{pmatrix} \ell & \ell_a & \ell_b \\ -m & m_a & m_b \end{pmatrix} \begin{pmatrix} \ell & \ell_c & \ell_d \\ -m & m_c & m_d \end{pmatrix} \langle \ell \|Y_{\ell_a}\| \ell_b\rangle^* \langle \ell' \|Y_{\ell_c}\| \ell_d\rangle \\
&\int R^*_{n_a \ell_a}(r)\, R^*_{n_b \ell_b}(r)\, \frac{1}{r^2} R_{n_c \ell_c}(r)\, R_{n_d \ell_d}(r)\, dr
\end{aligned} \tag{3.24}$$

The major ingredients for the complete study of ^{6}He are these matrix elements of pairing interaction. These correspond to the radial integrals and to the coefficients (calculated in Mathematica notebook mentioned in block 3 of procedure in appendix A and tabulated in chapter-5). Besides these important ingredients other vital factors are energy cuts and the completeness of the model space i.e. single-particle waves to be included in calculations. As we increase the model space i.e. number of basis states to be included, the calculations becomes computationally challenging and we need state-of-the-art data handling and software to process this large amount of data.

Chapter 4

Helium-5

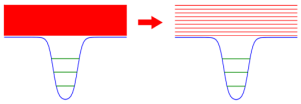

4.1 Initial remarks

The nucleus ^{4}He or an alpha particle is the only combination of four nucleons (two neutrons and two protons), which is bound. Moreover, ^{4}He is very strongly bound and the nucleons are paired to give a total spin $S = 0$. Interestingly, if we add a nucleon (either proton or neutron) to the alpha particle, we produce an unbound nucleus. Thus for $A = 5$ (^{5}Li or ^{5}He), we do not have bound nuclei [119].

The stability of light nuclei are greatly influenced by the variation of neutron number. This can be clearly seen in the isotopic chain of helium, where an increase in neutron number leads to the transformation of stable ^{4}He nucleus to unbound ^{5}He. Then we have weakly bound ^{6}He, unbound ^{7}He, weakly bound ^{8}He and unbound ^{9}He nucleus [109]. In order to study the weakly bound ^{6}He, we start from the description of the unbound subsystem. The subsystem ^{5}He is unbound, it exists only as a short-lived resonance that breaks up into the $\alpha + n$ channel. The known properties of the energy levels

Table 4.1: Energy levels of ^{5}He (from [119, 118].)

Excitation energy (MeV)	J^π; T	$\Gamma_{c.m.}$ (MeV)
g.s.	$\frac{3}{2}^-$; $\frac{1}{2}$	0.648
1.27	$\frac{1}{2}^-$; $\frac{1}{2}$	5.57
16.84	$\frac{3}{2}^+$; $\frac{1}{2}$	0.0745
19.14	$\frac{5}{2}^+$; $\frac{1}{2}$	3.56
19.26	$\frac{3}{2}^+$; $\frac{1}{2}$	3.96
19.31	$\frac{7}{2}^+$; $\frac{1}{2}$	3.02
19.96	$\frac{3}{2}^-$; $\frac{1}{2}$	1.92
21.25	$\frac{3}{2}^+$; $\frac{1}{2}$	4.61
21.39	$\frac{5}{2}^+$; $\frac{1}{2}$	3.95
21.64	$\frac{1}{2}^+$; $\frac{1}{2}$	4.03
23.97	$\frac{7}{2}^+$; $\frac{1}{2}$	5.44
24.06	$\frac{5}{2}^-$; $\frac{1}{2}$	5.23
(35.7±0.4)		≈ 2

of ^{5}He are shown in Fig. (4.1) and tabulated in Table − (4.1) [118, 119]. In Fig. (4.1), energy values are plotted vertically in MeV, with ground state fixed at zero.

The study of resonance structures in lighter nuclei, provides a rich source of information on many-body dynamics. Within the framework of scattering theory, resonances are studied both experimentally and theoretically by analyzing certain observables (cross sections, scattering amplitudes, phase shifts, etc.) at real energies. In scattering theory resonances are defined through the analytic properties of certain quantities (S matrix, Jost function etc.) at complex energies [107].

This chapter is organized as follows: In the section 4.2, we will discuss the various methods available in the market for dealing with continuum discretization. In the section 4.3, we will discuss the spectrum of ^{5}He along with phase shift analysis of ^{5}He resonances. Finally in section4.4, we will draw

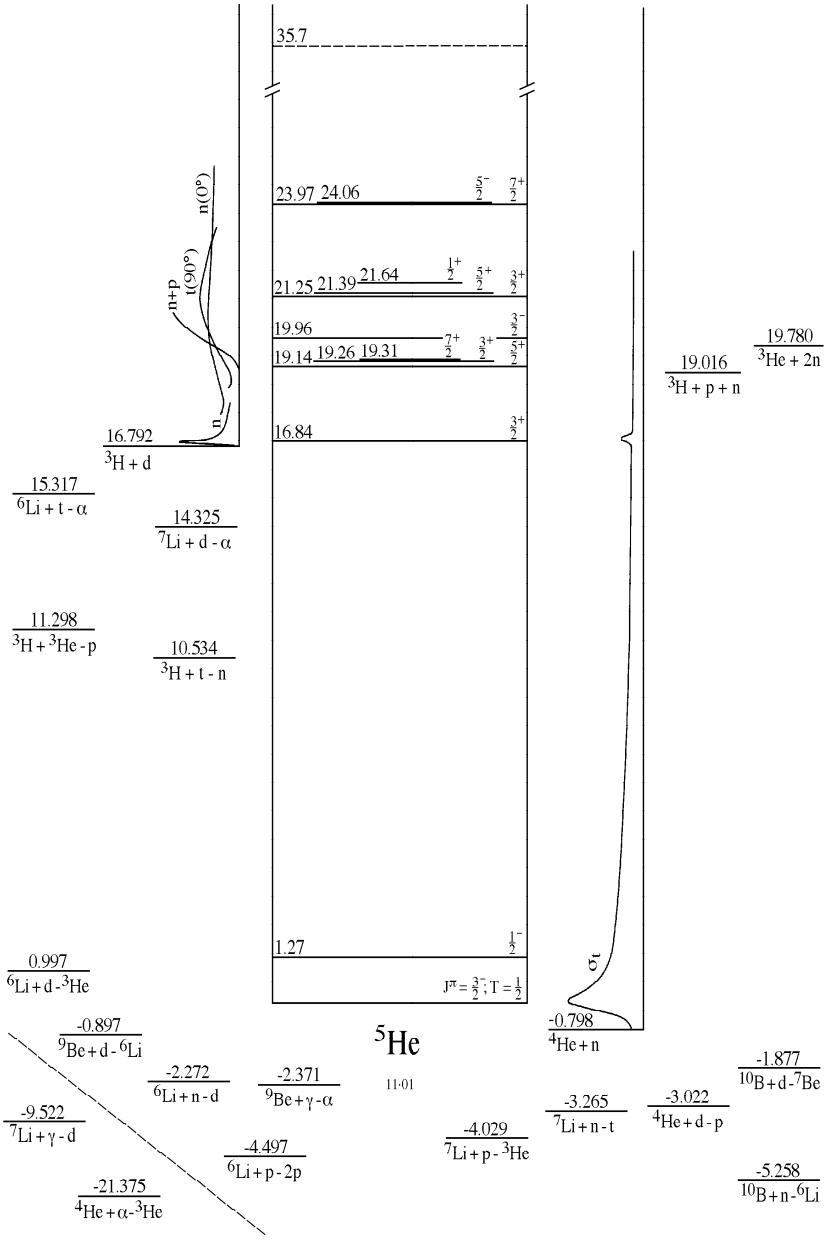

Figure 4.1: Energy levels of ^{5}He (from [119, 118].)

some conclusions.

4.2 Recipe to deal with Continuum discretization

The continuum wave functions are the functions of continuous variable i.e. the energy of continuum along with spatial variables. There are only few methods available to deal with continuum wave functions. In each method, the continuum wave function is approximated by finite set of square integrable functions. In literature there are two main methods, used so far for continuum discretization, namely bin method [110] and pseudo state method [111].

4.2.1 Bin method

In bin method, the continuum is discretized into a finite number of bins or set of energy intervals and the internal states within each bin are represented by a single wave function, which is constructed by superposition of true continuum wave functions within that bin. It is further categorized into two types, these are

1. The **mid-point method** [105, 110], is used in present calculations, which consists of taking scattering state

$$\tilde{\phi}_i(\vec{r}) = \sqrt{\Delta}\ \phi(\vec{r}, \bar{E}_i), \quad E_i > 0 \tag{4.1}$$

for discrete set of scattering energies, where $\bar{E}_i = (E_i + E_{i-1})/2$, with Δ as common energy interval or width of bin. In the mid-point method, continuum channels are represented by the channel at a midpoint of the bin. The resulting set of wavefunctions $\tilde{\phi}_{ij}(\vec{r})$ satisfies the following

orthogonality condition

$$\int \tilde{\phi}_i(\vec{r})\tilde{\phi}_j(\vec{r})d\vec{r} = \Delta\ \delta_{ij}\delta(\bar{E}_i - \bar{E}_j) \tag{4.2}$$

that depends on the bin width (Δ).

2. The **average method** [104, 105, 106, 108], where scattering wave functions $\tilde{\phi}_i(\vec{r})$ are averaged over an energy interval to make them square integrable and they are given by

$$\tilde{\phi}_i(\vec{r}) = \frac{1}{\sqrt{\Delta}} \int_{E_{i-1}}^{E_i} \phi(\vec{r}, E)dE\ . \tag{4.3}$$

In the average method the continuum channels within each bin are averaged into a single channel. The resulting set of wavefunctions $\tilde{\phi}_{ij}(\vec{r})$ satisfies the following orthogonality condition

$$\int \tilde{\phi}_i(\vec{r})\tilde{\phi}_j(\vec{r})d\vec{r} = \delta_{ij}\delta_{E_iE_j} \tag{4.4}$$

which is free from any explicit dependence on Delta (Δ).

4.2.2 Pseudo state method

In **pseudo-state method** [104, 111, 112], *pseudostates* are used, which are just the eigenstates of the internal Hamiltonian on some convenient square-integrable basis. A variety of pseudo states basis are available in literature for two-body continuum discretization [113, 114, 115] and also for three-body continuum [116, 117]. These pseudostates have the property to decay to zero at large distances. We will not discuss them on greater detail here, because they are not used in the present work.

4.3 Analysis of ^{4}He+n subsystem

Analysis of the ^{4}He+n subsystem (^{5}He) is indispensable in studying ^{6}He as a typical nucleus of Borromean system of ^{4}He+$n+n$. The interaction between ^{4}He and a valence neutron plays a vital role in the binding mechanism of ^{6}He. The shell model predicts a bound, completely filled, s state for the α core and an unbound p doublet, further split by spin-orbit interaction. Experimentally the $p_{3/2}$ and $p_{1/2}$ resonances are found at 0.789 MeV and 1.27 MeV above the neutron separation threshold [119, 118]. Their widths are quoted as 0.648 MeV and 5.57 MeV [119, 118] respectively. Note that these values have been extracted from raw data within R-matrix approach [119].

Theoretically, in order to extend the model space we have also included the $sd-$shell in the picture. The relative motion wave of the neutron with respect to the core is an unbound ($E_C > 0, k > 0$), oscillating dipole ($\ell = 1$) wave that must approximate a combination of spherical Bessel functions at large distances from the center. The continuum monopole ($\ell = 0$), dipole ($\ell = 1$) and quadrupole ($\ell = 2$) scattering single particle states ($E_C > 0, k > 0$) of ^{5}He are generated with Woods-Saxon (WS) potential given by

$$V_{WS} = \left[V_0 + V_{ls} r_0^2 (\vec{l}.\vec{s}) \frac{1}{r}\frac{d}{dr}\right] \left[1 + exp\left(\frac{r_0 - R}{a}\right)\right]^{-1} \tag{4.5}$$

Table 4.2: Woods-Saxon and spin-orbit potential parameters for ^{5}He.

V_0 (MeV)	r_0 (fm)	a (fm)	V_{ls} MeV
-42.6	1.2	0.9	8.5

For ^{5}He the parameter set used is tabulated in Table-4.2. The Woods-

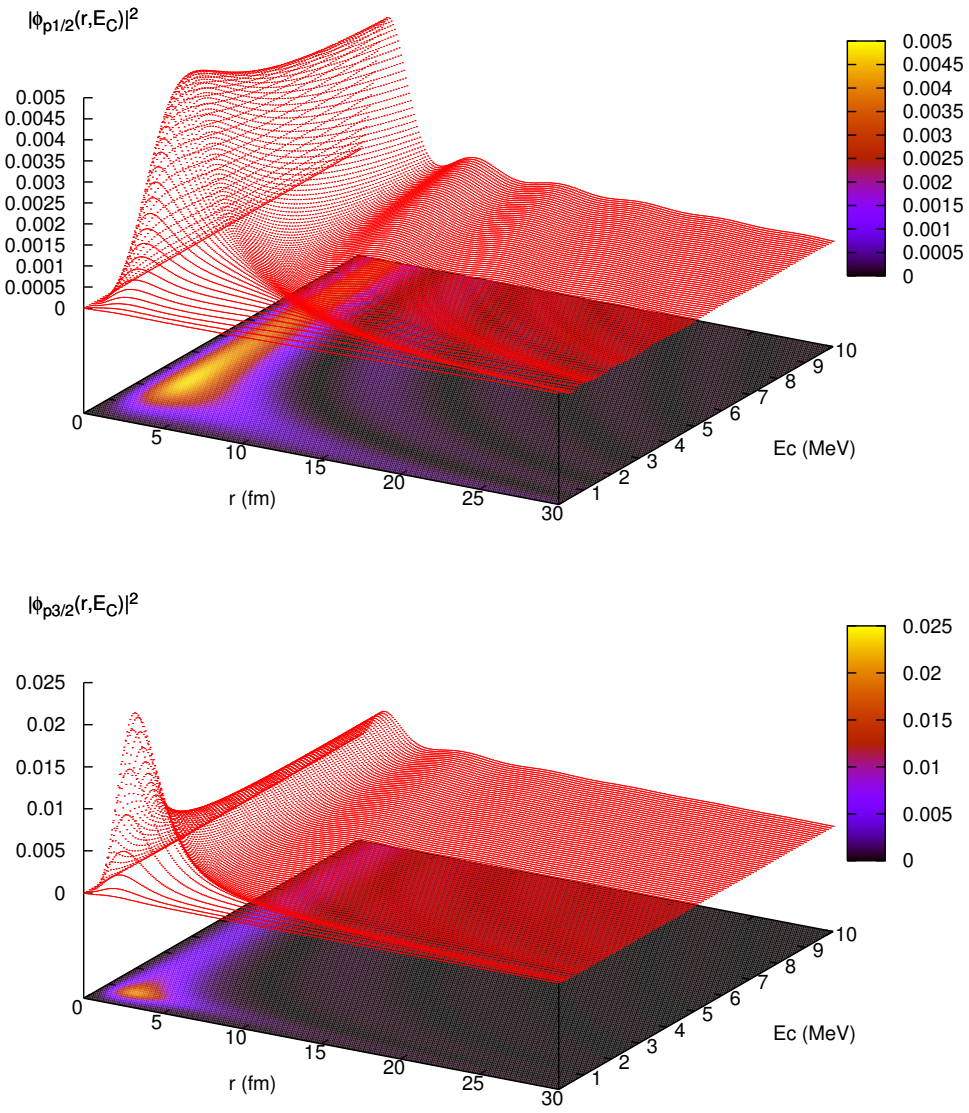

Figure 4.2: Calculated square of ^{5}He continuum wave functions (top: $p_{1/2}$, bottom: $p_{3/2}$) as a function of radial variable and continuum energy.

Saxon potential depth is $V_0 = -42.6$ MeV, while the geometric parameters are $r_0 = 1.2$ fm, $a = 0.9$ fm and the spin-orbit coefficient is $V_{ls} = 8.5$ MeV. The radial single-particle wavefunctions (as a function of continuum energy

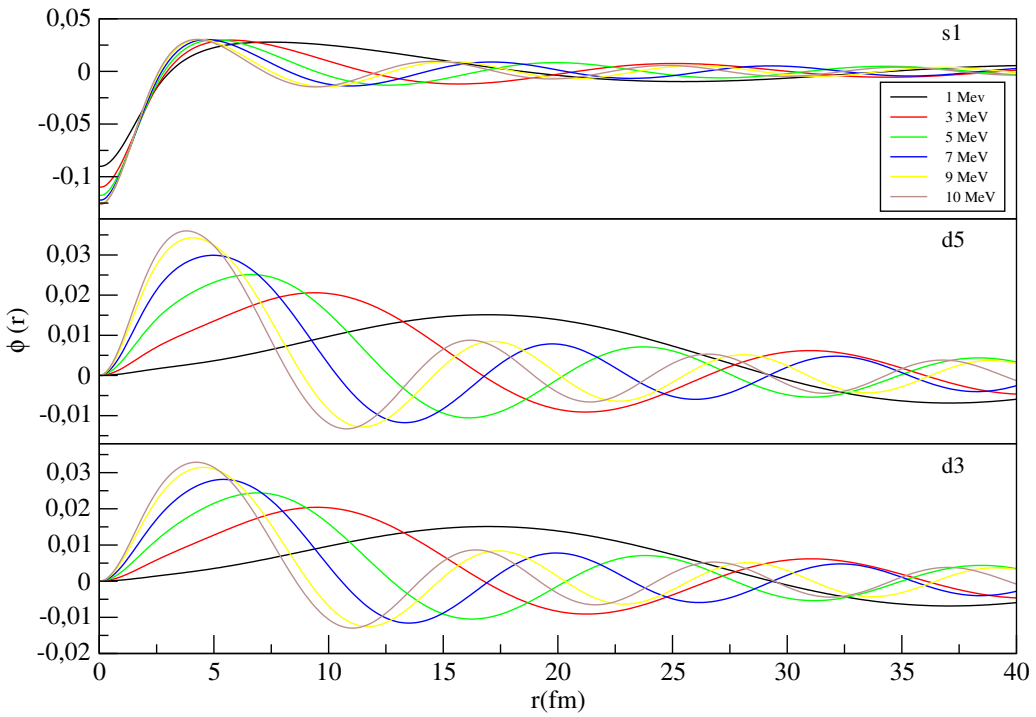

Figure 4.3: ^{5}He sd-continuum waves as a function of radial variable for continuum energies 1, 3, 5, 7, 9 and 10 MeV.

and radial coordinate) are obtained through the numerical integration, from the origin up to a cutoff distance, of radial Schrödinger equation, given by

$$-\frac{\hbar^2}{2\mu}\left[\frac{1}{r^2}\frac{d}{dr}(r^2\frac{d}{dr}) - \frac{l(l+1)}{r^2}\right]\phi(r,E_C) + V(r)\phi(r,E_C) = E\phi(r,E_C) \quad (4.6)$$

where $V(r)$ is the Woods-Saxon potential. The cutoff distance is the distance, beyond which potential is negligible, it exists if $rV(r) \to 0$ as $r \to \infty$. At cutoff distance, the inner solution is matched to the outer solution. This matching condition determines the radial single-particle wavefunctions, by making use of standard Coulomb functions, which reduces to Bessel functions for $Z = 0$. These *spd*−continuum single-particle states ($E_C > 0$) of ^{5}He are shown in Fig. (4.2) and Fig. (4.3), with energies from 0.1 to 10.0 MeV on a radial grid that goes from 0.1 to 30.0 fm and 40.0 fm respectively.

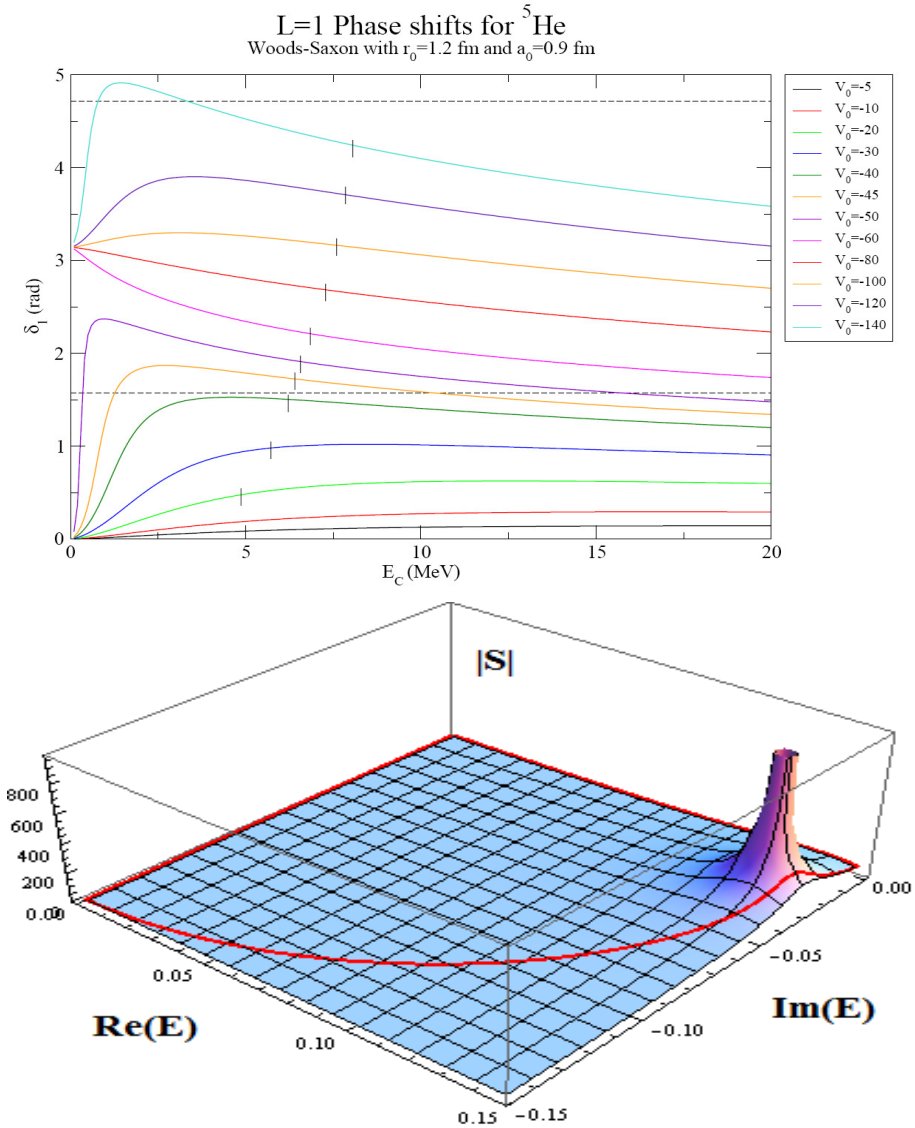

Figure 4.4: L= 1 phase shifts for ^{5}He. (Lower part) Countour integration (residues) on the S-matrix in the complex plane to pinpoint the position of the poles.

4.3.1 Phase shift and S-matrix analysis

With the aim of double-checking our results, we also did phase shift analysis to identify the resonances. In this case the width of resonance (Γ) is con-

nected to the first derivative of the phase shift (δ_l) and is given by relation

$$\Gamma = 2\left(\frac{d\delta_l}{dE}\right)^{-1} \tag{4.7}$$

The upper panel of Fig. (4.4), shows the $L = 1$ phase shifts for ^{5}He with different WS potential depths ranging from -5 to -140 MeV, with continuum energy from 0.1 to 20.0 MeV. The poles of the S-matrix have been calculated with the Jost functions for the WS + spin-orbit potentials. Using a different code, from the one used in previous subsection, the result is that, for $V_0 = -41.2$ MeV and $V_{ls} = 6.5$ MeV, one gets a $p_{3/2}$ resonance with real part 0.79 and imaginary part 0.49. The $p_{1/2}$ resonance comes at 1.27 MeV with a width of 1.62 MeV. It is clear from Fig. (4.1) and Table $-$ (4.1), the $p_{3/2}$ resonance is relative to n+^{4}He zero relative energy and $p_{1/2}$ resonance is related to energy of first resonance. Where as for $L = 0$ states, past studies [120, 121] shows the existence of s- virtual state, for scattering length of $3fm$. Most of the these calculations are interaction dependent. They claim that s- virtual state is unphysical and also has little impact on ^{6}He properties. The lower panel of Fig. (4.4), shows the poles of S-matrix in complex plane. Both calculations give similar outcomes, with similar parameters, although the widths are not in perfect agreement. Therefore for the sake of easing the following calculations, we will use the simpler results coming from the first approach.

4.4 Conclusions

It has been shown how *spd*$-$continuum single-particle states ($E_C > 0$) of ^{5}He are calculated with energies from 0.1 to 10.0 MeV on a radial grid that goes from 0.1 to 100.0 fm. Results are compared with more refined approaches,

giving confidence that we can use the calculated wavefunctions for constructing two-particle states in ^{6}He.

Chapter 5

Helium-6

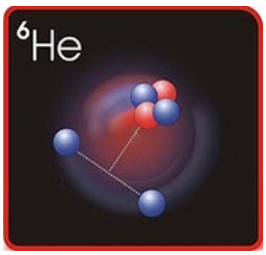

5.1 Initial remarks

Among neutron-rich nuclei, two-neutron halo nuclei (Borromean) are particularly intriguing systems to be investigated. Their structure has often been described as a three-body system consisting of two valence neutrons interacting with each other and with the core nucleus [38, 32, 95, 96, 91, 92]. The ^{6}He is the simplest Borromean nucleus, that serves as a ideal testing ground for few-body structure models. The nucleus ^{6}He is the system under probe, discussed in this thesis.

Despite of its early discovery [22], it still manages today to attract a large interest from the nuclear physics community in both theory and experiment. As compare to ^{11}Li ($E_{2n} = 0.25$ MeV) [48], the two-neutron separation energy of ^{6}He is larger ($E_{2n} = 0.97$ MeV), although this is still a very small with

Table 5.1: Energy levels of ^{6}He (from [119, 118].)

Excitation energy (MeV)	J^π; T	Decay
g.s.	0^+; 1	β^-
1.797±0.025	2^+; 1	n, α
5.6±0.3	(2^+, 1^-); 1	
14.6±0.7	(1^+, 2^-); 1	
(15.5±0.5)		
23.3±1.0		
(32)		
(36)		

respect to stable nuclei. The matter radii derived from interaction cross-sections, for $R_{rms}(^6\text{He})$ is $\sim$ 2.7 fm and for $R_{rms}(^{11}\text{Li})$ is $\sim$ 3.5 fm [2, 31], which is quite large as compare to the matter radii of respective cores i.e. for $R_{rms}(^4\text{He})$ is $\sim$ 1.5 fm and for $R_{rms}(^9\text{Li})$ is $\sim$ 2.3 fm. This further reveals that the wave function is less extended in ^{6}He than ^{11}Li. From the perspective of the extent of matter distribution, it is pretty much clear that ^{6}He is a $2n-$halo nucleus to a lesser extent than ^{11}Li.

^{6}He is a loosely bound Borromean nucleus with an extended neutron structure. The definite inclusion of this extended structure, in the theoretical study is often key to obtain a perfect agreement with the experiments. This three-body system can be pictured as being, in the two extreme cases, either an alpha particle and dineutron cluster, or a neutron-alpha-neutron chain (cigar) configuration. The ^{6}He is very well described by simple core + n + n model [94].

The known properties of the energy levels of ^{6}He are shown in Fig. (5.1) and tabulated in Table $-$ (5.1) [47, 119]. There are no bound excited states in ^{6}He and the two-neutron separation energy is 0.973 MeV. Among the resonances, only the 2^+ one at $E_x = 1.8$ MeV is well established.

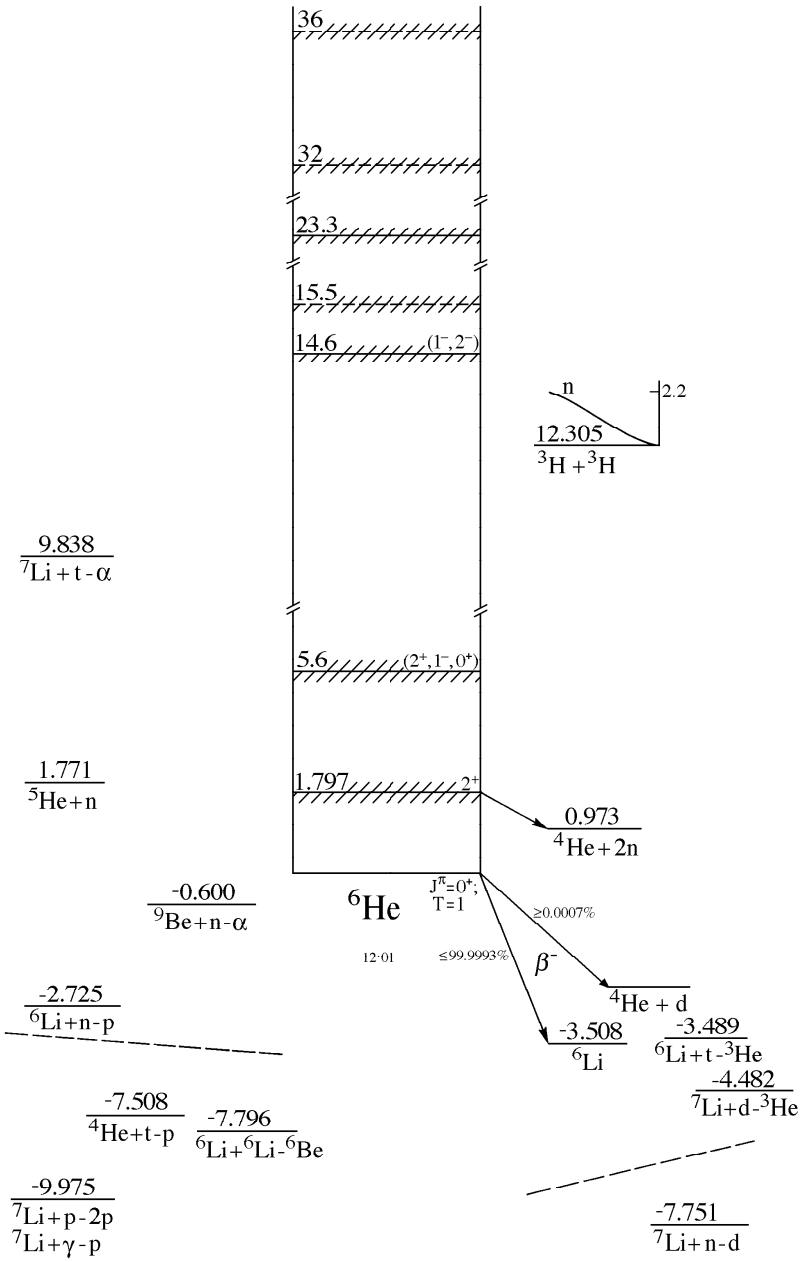

Figure 5.1: Energy levels of ^{6}He (from [119, 118].)

It is a sufficiently small system and can be used for testing various theoretical models, that can be compared to the experimental results. This chapter

Table 5.2: Possible configurations of ^{6}He arising from two neutrons in p-orbitals

	$p_{3/2}$	$p_{1/2}$
$p_{3/2}$	$0^+, 2^+$	$1^+, 2^+$
$p_{1/2}$		0^+

is organized as follows: In the section 5.2, we will discuss the various configurations arising from two neutrons in p-orbitals i.e. reduced model space. In the subsection 5.2.1, the necessity of full model space and not merely of p-states is discussed along the all possible configurations emerging from two neutrons in spd-orbitals. In section 5.3, we will discuss the eigenspectrum of ^{6}He along with variation of pairing strength with basis dimensions. In the section 5.4, we will discuss ground state properties of ^{6}He and their comparison with the earlier calculations. Finally in section5.5, we will draw some conclusions.

5.2 ^{6}He - reduced model space

The simple structure model, has been developed in order to study the weakly bound ground state and low-lying continuum states of Borromean nuclei, by coupling unbound waves of two-body subsystem. Initially it is tested for ^{6}He [82], with two non-interacting particles in the above single-particle levels of ^{5}He produces 5 positive-parity states when two neutrons are placed in the $p_{3/2}$ and $p_{1/2}$ unbound orbits. From Table $-$ (5.2), it is clear that two configurations namely $p^2_{3/2}$ and $p^2_{1/2}$ couple to $J = 0^+$, two configurations $p^2_{3/2}$ and $p_{3/2}p_{1/2}$ couple to $J = 2^+$ and only one configuration couples to $J = 1^+$. The unperturbed energies of $p^2_{3/2}$, $p_{3/2}p_{1/2}$ and $p^2_{1/2}$ configurations are 1.578, 2.06 and 2.54 MeV respectively, as indicated in the second column of Fig.(5.9). Fig. (5.9) also shows the 0^+ ground state of ^{6}He that is bound by 0.973

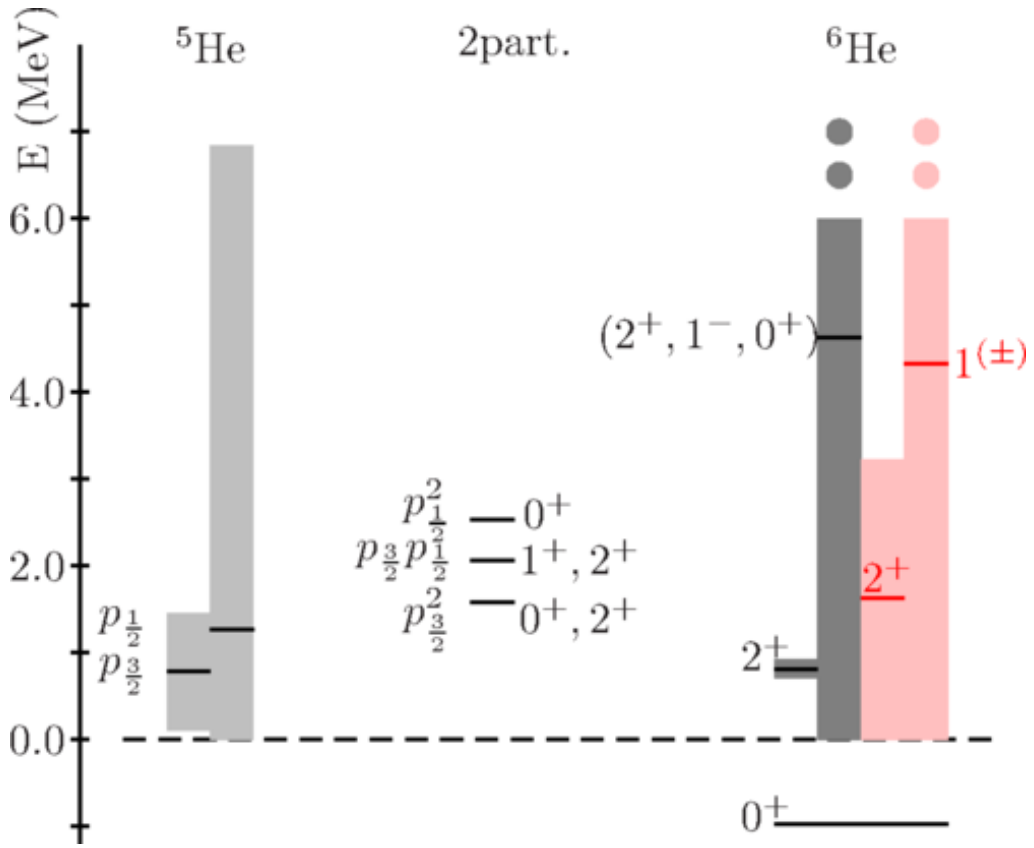

Figure 5.2: Left: experimental energy levels (resonances) in ^{5}He. Center: unperturbed energies of two particle states built upon the scheme on the left. Right: experimental energy levels (bound ground state and resonances) of ^{6}He. Shades of gray and pink indicate widths. The experimental energies are from Ref. [118] (in black) and Ref. [58] (in red). Parentheses indicate uncertain spin-parity assignment.

MeV and the 2^+ narrow resonant state found at 1.797 MeV ±25 keV above the ground state. According to standard databases another resonance is found at about 5.6 ±0.3 MeV with uncertain spin-parity assignment (given as $2^+, 1^-, 0^+$). No other states are present up to 14 MeV. The widths of these resonances are 113 ±20 keV (narrow 2^+) and 12.1 ±1.1 MeV (very broad) respectively. Notice that the mass of ^{6}He has been recently directly determined in the TITAN Penning trap at ISAC [90], showing important deviations at

the level of 4σ with respect to previous indirect measurements, reported also in the AME03 evaluation. Anyway, in absolute units, the 2-3 keV deviation of the newly determined 975.46(23) keV two-neutron separation energy is practically irrelevant to our scopes, because the level of precision of our calculation is about 0.5% in the g.s. case. Recent experimental observations [58], trying to disentangle the complicated nature of the ^{6}He continuum with the p(^{8}He,t) reaction at SPIRAL (GANIL), support the existence of two resonances above the neutron separation energy S_n: a 2^+ state at 2.6(3) MeV with Γ =1.6(4) MeV and a $1^{(+,-)}$ state at 5.3(3) MeV with Γ =2(1) MeV. These states are shown in red in Fig. (5.9). Several theories are listed in Ref. [58] and compared with the available experimental information. Most of them show the same set of levels that we have constructed on p orbitals.

5.2.1 Necessity for full model space

The somewhat puzzling nature of the excited states of ^{6}He has been also discussed recently in Ref. [84], where it is concluded that the spin and parity of the 5.3 MeV state is most probably 0^+, in contrast with the analysis proposed with the experimental data. Our simple scheme is confirmed by *ab initio* theories [83, 58] (at the level of 12 $\hbar\omega$) find the sequence of levels $(0^+, 2^+, 2^+, 1^+, 0^+)$ with a third 0^+ lowering rapidly as the basis is increased (see Fig.1 of cited Ref. [83]). If the 1^- attribution of part of the strength is confirmed, then *its nature cannot be associated with 2 neutrons sitting in p orbitals.* One might wonder whether dipole strength should be present: certainly a highly collective dipole mode built at high excitation energy as a coherent superposition of p-h states must exist, but its nature in ^{6}He calls for promotion of one neutron from the p to the sd shell. The low-energy tail of this giant dipole resonance indeed is expected to come down till zero

Table 5.3: Possible configurations of ^{6}He arising from two neutrons in s-, p- and d-orbitals

	$s_{1/2}$	$p_{1/2}$	$p_{3/2}$	$d_{3/2}$	$d_{5/2}$
$s_{1/2}$	0^+	$0^-, 1^-$	$1^-, 2^-$	$1^+, 2^+$	$2^+, 3^+$
$p_{1/2}$		0^+	$1^+, 2^+$	$1^-, 2^-$	$2^-, 3^-$
$p_{3/2}$			$0^+, 2^+$	$0^-, 1^-, 2^-, 3^-$	$1^-, 2^-, 3^-, 4^-$
$d_{3/2}$				$0^+, 2^+$	$1^+, 2^+, 3^+, 4^+$
$d_{5/2}$					$0^+, 2^+, 4^+$

and therefore it might mix significantly with other states and make the spin-parity assignment very difficult. This strength might also come from other configurations, such as $\alpha + (2n)$ cluster configurations, that mix with the $\alpha + n + n$ configuration. Later on we have performed extended calculations, by including $sd-$shell also in the theoretical formalism [97, 98, 99]. The simple model with two non-interacting particles in the above single-particle levels of ^{5}He produces different parity states, when two neutrons are placed in five different unbound orbits, $s_{1/2}$, $p_{1/2}$, $p_{3/2}$, $d_{3/2}$ and $d_{5/2}$. Namely five configurations $(s_{1/2})^2$, $(p_{1/2})^2$, $(p_{3/2})^2$, $(d_{3/2})^2$ and $(d_{5/2})^2$ couple to $J = 0^+$, seven configurations $(s_{1/2}d_{3/2})$, $(s_{1/2}d_{5/2})$, $(p_{1/2}p_{3/2})$, $(p_{3/2}p_{3/2})$, $(d_{3/2}d_{3/2})$, $(d_{3/2}d_{5/2})$ and $(d_{5/2}d_{5/2})$ couple to $J = 2^+$, five configurations $(s_{1/2}p_{1/2})$, $(s_{1/2}p_{3/2})$, $(p_{1/2}d_{3/2})$, $(p_{3/2}d_{3/2})$ and $(p_{3/2}d_{5/2})$ couple to $J = 1^-$ and three configurations $(p_{1/2}d_{5/2})$, $(p_{3/2}d_{3/2})$ and $(p_{3/2}d_{5/2})$ couple to $J = 3^-$. Other less important multipolarities can also be constructed see Table $-$ (5.3).

In Table $-$ (A.1), the number of configurations are tabulated corresponding to all possible natural and non-natural parity J^π states. From Table $-$ (A.1) it is clear that calculations for ground state 0^+ and excited 1^- and 2^+ states are computationally challenging because they arise from many different configurations, $5, 5$ and 7 configurations respectively. For 3^- calculations are relatively fast as it emerges from only three configurations. We have not included non-natural parity states in this study, although in principles we

Table 5.4: Total number of configurations coupling to each J^π

J^π	No. of configurations	J^π	No. of configurations
0^+	5	0^-	2
1^-	5	1^+	3
2^+	7	2^-	5
3^-	3	3^+	2
4^+	2	4^-	1

have all the ingredients to do it.

5.3 Eigenspectrum of ^{6}He

The five states of ^{5}He are not discrete, but rather depend on the energies of the continuum orbitals. Each single particle continuum wavefunction is given by

$$\phi_{\ell,j,m}(\vec{r}, E_C) = \phi_{\ell,j}(r, E_C)[Y_{\ell m_\ell}(\Omega) \times \chi_{1/2,m_s}]^{(j)}_m \tag{5.1}$$

with $E_C > 0$. These are used as building blocks to form a basis for ^{6}He states. The combined tensor product of these two is given by

$$\psi_{JM}(\vec{r}_1, \vec{r}_2) = [\phi_{\ell_1,j_1,m_1}(\vec{r}_1, E_{C1}) \times \phi_{\ell_2,j_2,m_2}(\vec{r}_2, E_{C2})]^{(J)}_M \tag{5.2}$$

In LS-coupling for $\ell_1 \neq \ell_2$ the antisymmetric wavefunction $\psi\left(\ell_1\ell_2SLJM\right)$ is given by

$$\begin{aligned}\psi\left(\ell_1\ell_2SLJM\right) = \frac{1}{\sqrt{2}} \sum_{M_S,M_L} \langle SM_SLM_L|SLJM\rangle \times \\ [\phi_{12}(\ell_1\ell_2LM_L)\chi_{12}(s_1s_2SM_S) - \phi_{21}(\ell_2\ell_1LM_L)\chi_{21}(s_2s_1SM_S)]\end{aligned} \tag{5.3}$$

where we have dropped the dependence on $\vec{r}_1$ and $\vec{r}_2$ for simplicity. We take an attractive pairing contact delta interaction for simplicity, although, as

it is well-known, density dependent interactions might be more appropriate [101, 102]. The explicit expression for V_{12} is given by

$$V_{12} = -g\delta\left(r_1 - r_2\right) \tag{5.4}$$

where

$$\delta\left(r_1 - r_2\right) = \frac{1}{r_1 r_2}\delta\left(r_1 - r_2\right)\delta\left(cos\theta_1 - cos\theta_2\right)\delta\left(\varphi_1 - \varphi_2\right) \tag{5.5}$$

The major ingredients for the complete study of ^{6}He are the matrix elements of pairing interaction. The matrix elements due to mutual interaction V_{12} in LS-coupling of two particles are given by

$$\begin{aligned}
&\langle \ell_a \ell_b S L J M | V_{12} | \ell_c \ell_d S' L' J' M' \rangle = \\
&\sum \langle S M_S L M_L | S L J M \rangle \langle S' M'_S L' M'_L | S' L' J' M' \rangle \\
&\langle s_1 m_{s_1} s_2 m_{s_2} | s_1 s_2 S M_S \rangle \langle s'_1 m'_{s_1} s'_2 m'_{s_2} | s'_1 s'_2 S' M'_S \rangle \\
&\langle \ell_a m_a \ell_b m_b | \ell_a \ell_b L M_L \rangle \langle \ell_c m_c \ell_d m_d | \ell_c \ell_d L' M'_L \rangle \\
&\sum_{\ell m} (-1)^{2(\ell - m)} \begin{pmatrix} \ell & \ell_a & \ell_b \\ -m & m_a & m_b \end{pmatrix} \begin{pmatrix} \ell & \ell_c & \ell_d \\ -m & m_c & m_d \end{pmatrix} \\
&\langle \ell \| Y_{\ell_a} \| \ell_b \rangle^* \langle \ell' \| Y_{\ell_c} \| \ell_d \rangle \\
&\int R^*_{n_a \ell_a}(r)\, R^*_{n_b \ell_b}(r)\, \frac{1}{r^2} R_{n_c \ell_c}(r)\, R_{n_d \ell_d}(r)\, dr
\end{aligned} \tag{5.6}$$

where R_{nl}'s are the single-particle radial wave functions. These correspond to the radial integrals also called Slater integrals and to the coefficients. For ground state these coefficients are used for calculation of contribution of various configurations and some ground state properties. The coefficients of these matrix elements of eq. (5.6) for $0^+, 1^-, 2^+$ and 3^- are summarized in Tables – (5.5, 5.6, 5.7 and 5.8) below. These calculations will lead to

Table 5.5: Coefficients of the ground state (0^+) of ^{6}He

$s_1s_1 - s_1s_1$ $1/2\pi$	$s_1s_1 - p_1p_1$ $-1/2\pi$	$s_1s_1 - p_3p_3$ $-1/\sqrt{2}\pi$	$s_1s_1 - d_3d_3$ $1/\sqrt{2}\pi$	$s_1s_1 - d_5d_5$ $\sqrt{3}/2\pi$
	$p_1p_1 - p_1p_1$ $1/2\pi$	$p_1p_1 - p_3p_3$ $1/\sqrt{2}\pi$	$p_1p_1 - d_3d_3$ $-1/\sqrt{2}\pi$	$p_1p_1 - d_5d_5$ $-\sqrt{3}/2\pi$
		$p_3p_3 - p_3p_3$ $1/\pi$	$p_3p_3 - d_3d_3$ $-1/\pi$	$p_3p_3 - d_5d_5$ $-\sqrt{3/2}/\pi$
			$d_3d_3 - d_3d_3$ $1/\pi$	$d_3d_3 - d_5d_5$ $\sqrt{3/2}/\pi$
				$d_5d_5 - d_5d_5$ $3/2\pi$

Table 5.6: Coefficients of the 1^- of ^{6}He

$s_1p_1 - s_1p_1$ $1/6\pi$	$s_1p_1 - s_1p_3$ $1/3\sqrt{2}\pi$	$s_1p_1 - p_1d_3$ $-1/3\sqrt{2}\pi$	$s_1p_1 - p_3d_3$ $2/3\sqrt{10}\pi$	$s_1p_1 - p_3d_5$ $-1/\sqrt{10}\pi$
	$s_1p_3 - s_1p_3$ $1/3\pi$	$s_1p_3 - p_1d_3$ $-1/3\pi$	$s_1p_3 - p_3d_3$ $1/3\sqrt{5}\pi$	$s_1p_3 - p_3d_5$ $-1/\sqrt{5}\pi$
		$p_1d_3 - p_1d_3$ $1/3\pi$	$p_1d_3 - p_3d_3$ $-1/3\sqrt{5}\pi$	$p_1d_3 - p_3d_5$ $1/\sqrt{5}\pi$
			$p_3d_3 - p_3d_3$ $1/15\pi$	$p_3d_3 - p_3d_5$ $-1/5\pi$
				$p_3d_5 - p_3d_5$ $3/2\pi$

the calculation of higher excited states in low-lying continuum of ^{6}He. For all these states the coefficients of matrix elements are calculated for upper diagonal part of the matrix only due to symmetry.

It is clear that one needs at least to introduce the residual interaction between continuum states, a task that requires careful numerical implementation because one deals with large datasets. We have calculated the continuum single-particle wave functions, with energies from 0.0 to 10.0 MeV, normalized to a delta similarly to Ref. [103], for the p-states of ^{5}He on a radial grid that goes from 0.1 fm to 100.0 fm with the potential discussed

Table 5.7: Coefficients of the 2^+ of ^{6}He

$s_1d_3 - s_1d_3$ $1/6\pi$	$s_1d_3 - s_1d_5$ $-\sqrt{3/2}/5\pi$	$s_1d_3 - p_1p_3$ $-1/5\pi$	$s_1d_3 - p_3p_3$ $-1/5\pi$	$s_1d_3 - d_3d_3$ $1/5\pi$	$s_1d_3 - d_3d_5$ $\sqrt{3/7}/5\pi$	$s_1d_3 - d_5d_5$ $2\sqrt{3/7}/5\pi$
	$s_1d_5 - s_1d_5$ $3/10\pi$	$s_1d_5 - p_1p_3$ $\sqrt{3/2}/5\pi$	$s_1d_5 - p_3p_3$ $\sqrt{3/2}/5\pi$	$s_1d_5 - d_3d_3$ $-\sqrt{3/2}/5\pi$	$s_1d_5 - d_3d_5$ $-3/5\sqrt{14}\pi$	$s_1d_5 - d_5d_5$ $-3\sqrt{2/7}/5\pi$
		$p_1p_3 - p_1p_3$ $1/5\pi$	$p_1p_3 - p_3p_3$ $1/5\pi$	$p_1p_3 - d_3d_3$ $-1/5\pi$	$p_1p_3 - d_3d_5$ $-\sqrt{3/7}/5\pi$	$p_1p_3 - d_5d_5$ $-2\sqrt{3/7}/5\pi$
			$p_3p_3 - p_3p_3$ $1/5\pi$	$p_3p_3 - d_3d_3$ $-1/\pi$	$p_3p_3 - d_3d_5$ $-\sqrt{3/7}/5\pi$	$p_3p_3 - d_5d_5$ $-2\sqrt{3/7}/5\pi$
				$d_3d_3 - d_3d_3$ $1/5\pi$	$d_3d_3 - d_3d_5$ $\sqrt{3/7}/5\pi$	$d_3d_3 - d_5d_5$ $2\sqrt{3/7}/5\pi$
					$d_3d_5 - d_3d_5$ $3/35\pi$	$d_3d_5 - d_5d_5$ $6/35\pi$
						$s_1d_3 - d_5d_5$ $12/35\pi$

Table 5.8: Coefficients of the 3^- of ^{6}He

$p_1d_5 - p_1d_5$ $3/14\pi$	$p_1d_5 - p_3d_3$ $-3\sqrt{3/10}/7\pi$	$p_1d_5 - p_3d_5$ $3/7\sqrt{5}\pi$
	$p_3d_3 - p_3d_3$ $9/35\pi$	$p_3d_3 - p_3d_5$ $-3\sqrt{6}/35\pi$
		$p_3d_5 - p_3d_5$ $6/35\pi$

above (Notice that this amount to 2.4 Gb of data for each component). With these wave functions, using the mid-point method with an energy spacing of 2.0, 1.0, 0.5, 0.2 and 0.1 MeV, corresponding to block basis dimensions of N =5, 10, 20, 50 and 100 respectively, we formed the two particle states and calculated the matrix elements of the pairing interaction ($\sim$ 4Gb of data for the largest case). This has been diagonalized with standard routines and it has given the eigenvalues shown in Fig. (5.3) for the $J = 0$ case with two neutrons in p- orbitals and in Fig. (5.4) for the $J = 0$ case with two neutrons in spd- orbitals. It is clear from Fig. (5.4) that, with an increase in basis dimensions the superfluous bound states appearing for $N = 5$ and 10 move into the continuum as expected. The coefficient of the $\delta-$contact matrix, G, has been adjusted to reproduce the correct ground state energy each time. The actual pairing interaction g is obtained by correcting with a factor that depends on the aforementioned spacing between energy states and it is practically a constant, except for the smallest basis. These quantities are also reported in Fig. (5.3) and (5.4) (panels on the right). Notice that the biggest adopted basis size gives a fairly dense continuum in the region of interest.

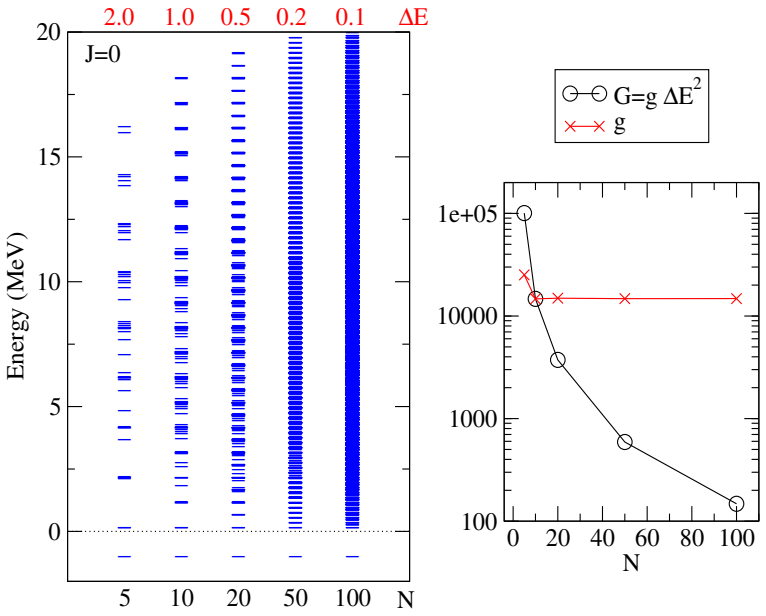

Figure 5.3: Left: Eigenspectrum of the interacting two-particle case for $J = 0$ with two neutrons sitting in p- orbitals (i.e. reduced model space) for increasing basis dimensions, N. The coefficient of the $\delta-$contact matrix, G, has been adjusted each time to reproduce the g.s. energy (right). The actual strength of the pairing interaction, g, is obtained by correcting with the energy spacing ΔE (also reported in red in the left part) and it is practically a constant.

5.4 Ground state properties

The radial part of the $S = 0$ ground state wavefunction obtained from the diagonalization in the largest basis ($N = 100$) is displayed in the upper part of Fig.(5.5). Due to symmetry reasons and to the fact that $\ell_1 = \ell_2 = 1$, there is no $S = 1$ component for a $\delta-$interaction (see Ref. [100], ch. 20). In fact, in this case, we can write the two-particle wavefunction as $\Psi(\vec{r}_1, \vec{r}_2) = \Psi(r_1, r_2)\mathscr{Y}^+_{JM}(\Omega_1, \Omega_2)\chi_{S=0}$. It is symmetric with respect to the exchange of coordinates of the two identical neutrons. It shows a certain degree of collectivity, taking contributions of comparable magnitude (though

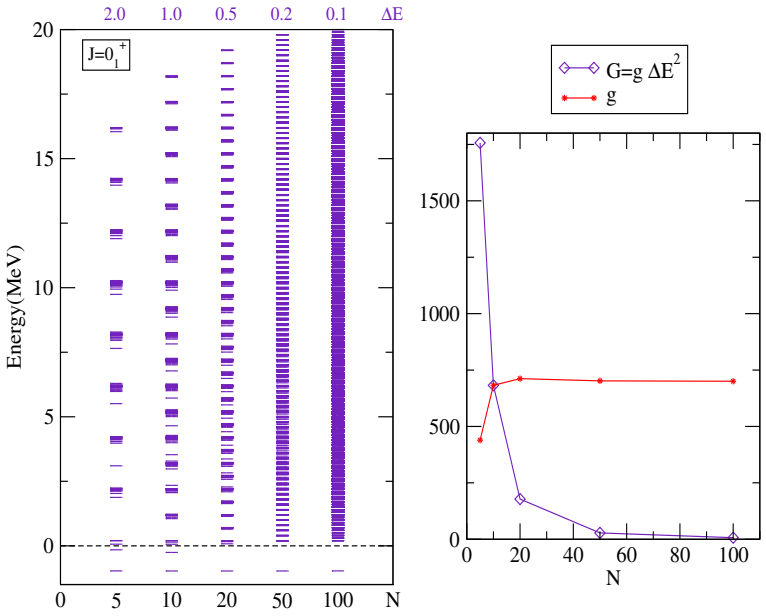

Figure 5.4: Left: Eigenspectrum of the interacting two-particle case for $J = 0$ with two neutrons sitting in spd- orbitals (i.e. full model space) for increasing basis dimensions, N. The coefficient of the $\delta-$contact matrix, G, has been adjusted each time to reproduce the g.s. energy (right). The actual strength of the pairing interaction, g, is obtained by correcting with the energy spacing ΔE and it is practically a constant.

not all of the same sign) from several basis states, while in contrast the remaining unbound states usually are made up of a few major components. The surface plot shows the exponential behavior at large r_1 and r_2 typical of a bound state, despite being the sum of many products of oscillating wave functions. In Fig. (5.5) one can also see, especially from the contour plot located at the bottom, that the ground state wavefunction is symmetric with respect to exchange of r_1 and r_2. One can see from the bottom part of the figure that the square of the amplitudes of the $(p_{3/2})^2$ components are dominant summing up to 97.2%. In principle also the sd-continuum should be introduced in the picture, because the $(s_{1/2})^2$ $(d_{5/2})^2$ and $(d_{3/2})^2$configurations of course couple to $J = 0$. Therefore we introduced the sd- shell and did the

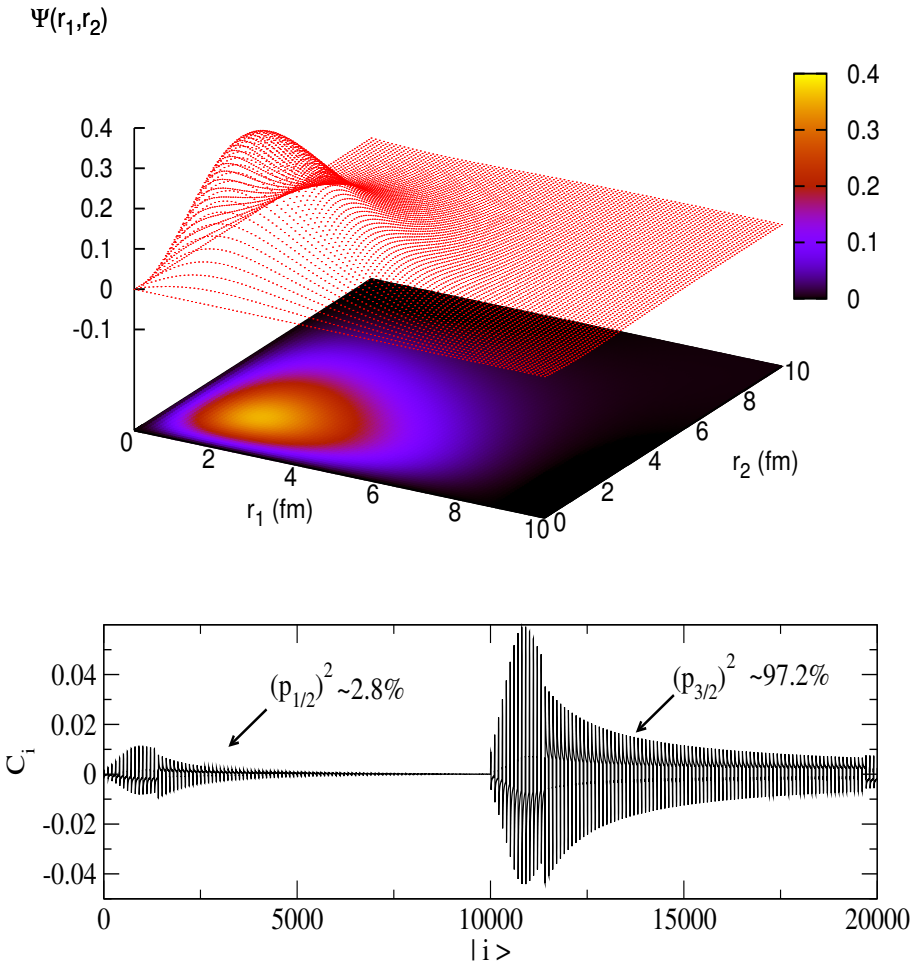

Figure 5.5: Ground state wave function ($S = 0$) for N =100 as a function of the coordinates of the two neutrons and corresponding contour plot (upper part). Decomposition of the g.s. into the J=0 basis (lower part) as a function of an arbitrary basis state label: the basis is divided in two blocks, 10^4 $[p_{1/2} \times p_{1/2}]^{(0)}$ components and then 10^4 $[p_{3/2} \times p_{3/2}]^{(0)}$ components (i.e. reduced model space). The ordering in each block is established by the sequential energies of each pair of continuum s.p. states, i.e. (E_{C_1}, E_{C_2}) = (0.1, 0.1), (0.1, 0.2), ... ,(0.1, 10.0), (0.2, 0.1), (0.2, 0.2), ... (10.0, 10.0).

challenging numerical computations. One can see from the Fig. (5.6) that

Table 5.9: Components of the ground state (0^+) of ^{6}He

Config.	Present	T.Myo[122]	Hagino[77]
$(2s_{1/2})^2$	0.008	0.009	–
$(1p_{1/2})^2$	0.080	0.043	–
$(1p_{3/2})^2$	0.897	0.917	0.830
$(1d_{3/2})^2$	0.005	0.007	–
$(1d_{5/2})^2$	0.009	0.024	–

the square of the amplitudes of the $(p_{3/2})^2$ components in this case are still dominant summing up to 89.7%. The precise percentage of each component is summarized in Table − 5.9, and compared with the previous calculations of T.Myo [122] and Hagino [77]. Present calculations are well in agreement with previous calculations. While the calculations by Hagino are made more or less in same fashion. Notice that, in our approach, there is no information on the angular correlation, that has nevertheless been extensively investigated by various authors: it corresponds to the $\mathscr{C}_{\ell^2;00}(\theta_{12})$ of Ref. [75].

In Table − (5.10), a number of calculated ground state properties are compared with earlier studies [122, 77], where R_m is the matter radius,

$$\langle r_{NN}\rangle = \langle\psi_{gs}(\vec{r}_1,\vec{r}_2)|(\vec{r}_1-\vec{r}_2)^2|\psi_{gs}(\vec{r}_1,\vec{r}_2)\rangle \tag{5.7}$$

is the mean square distance between the valence neutrons, and

$$\langle r_{c-NN}\rangle = \langle\psi_{gs}(\vec{r}_1,\vec{r}_2)|(\vec{r}_1+\vec{r}_2)^2/4|\psi_{gs}(\vec{r}_1,\vec{r}_2)\rangle \tag{5.8}$$

is the mean square distance of their center of mass with respect to the core.

It is also very important to evaluate the two-particle density of ^{6}He as a function of two radial coordinates, r_1 and r_2, for valence neutrons, and the angle between them, θ_{12} in LS-coupling scheme that is given by

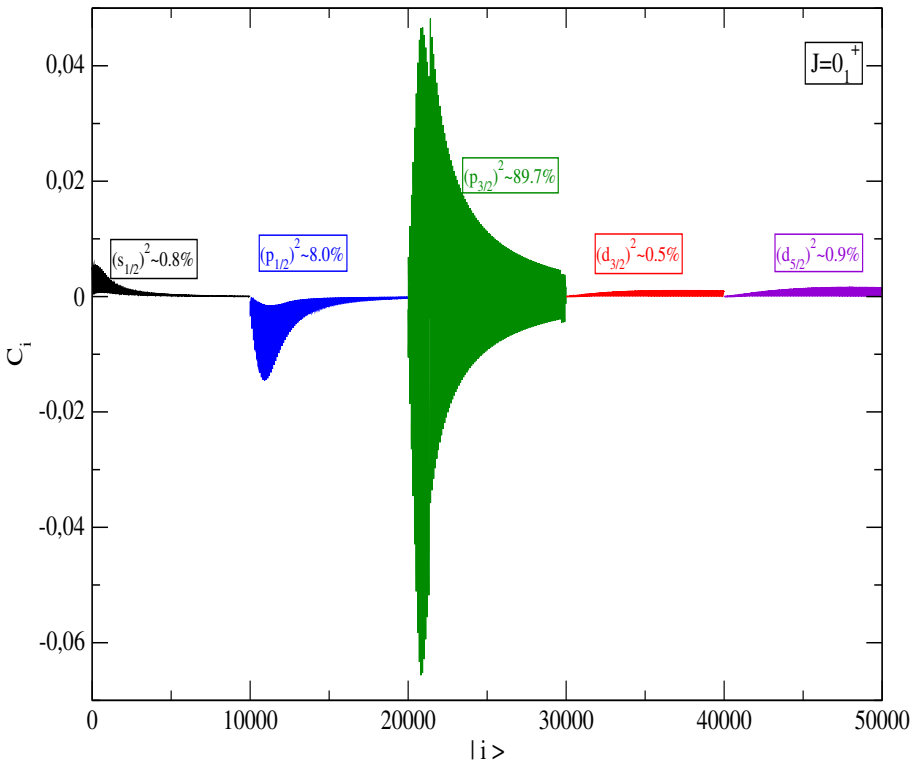

Figure 5.6: Decomposition of the g.s. into the J=0 basis as a function of an arbitrary basis state label $|i>$: the basis is divided into five blocks, 10^4 $[s_{1/2} \times s_{1/2}]^{(0)}$, 10^4 $[p_{1/2} \times p_{1/2}]^{(0)}$, 10^4 $[p_{3/2} \times p_{3/2}]^{(0)}$, 10^4 $[d_{3/2} \times d_{3/2}]^{(0)}$ and 10^4 $[d_{5/2} \times d_{5/2}]^{(0)}$ components (i.e. full model space). The ordering in each block is established by the sequential energies of each pair of continuum s.p. states, i.e. $(E_{C_1}, E_{C_2}) = (0.1, 0.1)$, $(0.1, 0.2)$, ... ,$(0.1, 10.0)$, $(0.2, 0.1)$, $(0.2, 0.2)$, ... $(10.0, 10.0)$. Compare this picture reporting the percentage in the full model space with the previous one, obtained with the p-shell only.

Table 5.10: Radial properties of the ground state of ^{6}He in units of fm

	Present	T.Myo[122]	Hagino[77]
R_m	2.37674	2.37	...
r^2_{NN}	28.8404	23.2324	21.3
r^2_{c-2N}	7.21011	9.9225	13.2

$$\rho(r_1, r_2, \theta_{12}) = \rho^{S=0}(r_1, r_2, \theta_{12}) + \rho^{S=1}(r_1, r_2, \theta_{12}) \tag{5.9}$$

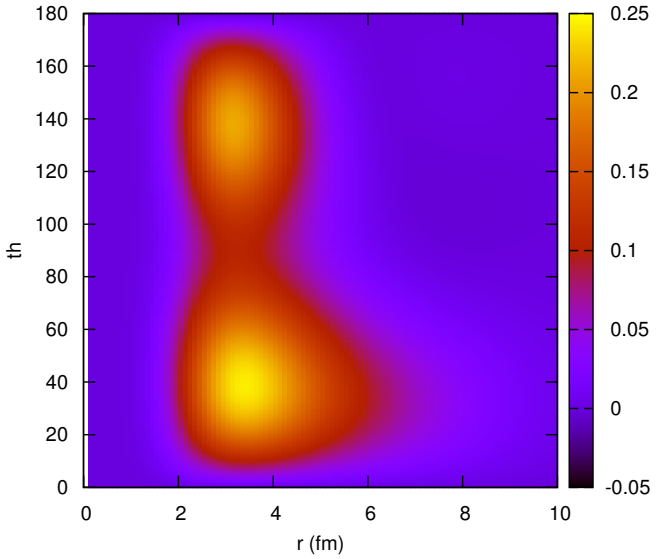

Figure 5.7: Two particle density (in full model space) for ^{6}He as a function of $r_1 = r_2 = r$ and angle between the valence neutrons θ_{12}.

The explicit expression for $S = 0$ component is given by [38]

$$\begin{aligned}\rho^{S=0}(r_1, r_2, \theta_{12}) = \quad & \frac{1}{8\pi} \sum_L \sum_{\ell,j} \sum_{\ell',j'} \frac{\hat{\ell}\hat{\ell}'\hat{L}}{\sqrt{4\pi}} \begin{pmatrix} \ell & \ell' & L \\ 0 & 0 & 0 \end{pmatrix}^2 \\ & \times \psi_{\ell j}(r_1, r_2) \psi_{\ell' j'}(r_1, r_2) Y_{L0}(\theta_{12}) \\ & \times (-1)^{\ell+\ell'} \sqrt{\frac{2j+1}{2\ell+1}} \sqrt{\frac{2j'+1}{2\ell'+1}} \end{aligned} \tag{5.10}$$

where $\hat{\ell} = \sqrt{2l+1}$ and $\psi_{\ell j}(r_1, r_2)$ is the radial part of two-particle wavefunc-

tion given by

$$\psi_{\ell j}(r_1, r_2) = \sum_{n2 \leq n1} \frac{\alpha_{n_1 n_2 \ell j}}{\sqrt{2(1+\delta_{n_1 n_2})}} \times(\phi_{n_1 \ell j}(r_1)\phi_{n_2 \ell j}(r_2) + \phi_{n_1 \ell j}(r_2)\phi_{n_2 \ell j}(r_1)) \quad (5.11)$$

where n_1 and n_2 are radial quantum numbers and $\alpha_{n_1 n_2 \ell j}$ is an expansion coefficient. Fig. (5.7) shows the two-particle density plotted as a function of the radius $r_1 = r_2 \equiv r$ and the angle θ_{12}, and with a weight factor of $4\pi r^2 \cdot 2\pi r^2 \sin\theta_{12}$. As it has been pointed out in [77], one observes two peaks in the two particle densities. The peak at smaller and larger θ_{12} are referred to as "di-neutron"and "cigar-like"configurations respectively. In this case the di-neutron component has a slightly higher density and it has a longer radial tail, which confirms the halo structure of ^{6}He, while the cigar-like component has a very compact structure comparatively. The percentage contribution of di-neutron configuration is $\sim$ 64% and whereas the cigar component has $\sim$ 36% contribution.

5.5 Conclusions

It has been shown how the bound halo ground state of ^{6}He emerges from the coupling of five unbound spd- waves in the continuum of ^{5}He, due to presence of pairing interaction. Contribution of different configurations has been presented and we can conclude that the dineutron configuration is slightly more favored over the cigar one. Radial properties of ground state of ^{6}He are also presented and compared with other calculations showing good agreement.

Chapter 6

Electromagnetic response of ^{6}He

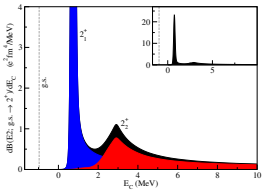

6.1 Initial remarks

The weakly bound nature of nuclei along the neutron drip line, leads to the concentration of multipole strength (of monopole, dipole, quadrupole, octupole etc. nature) at excitation energies above the continuum threshold. Within a simple crude three body structure model [82, 97, 98, 99], the weakly bound ground state and low-lying continuum states of ^{6}He are set by coupling two unbound spd-waves of ^{5}He. With all these necessary ingredients (presented in chapter−5), we have investigated the electric transitions to the continuum : the monopole, dipole, quadrupole and octupole response of the system and contributions of different configurations to these electric multipoles has been discussed. Due to the limitation of computation time, the monopole, dipole and octupole response of ^{6}He are investigated in full model space and quadrupole response of the system is investigated in reduced

model space. This chapter is organized as follows. In the section 6.2, we will present the investigation of pairing strength for all different multipolarities. In the section 6.3, we will set up the formulation of electric transitions to continuum. In the section 6.4, we will discuss the quadrupole response in reduced model space for ^{6}He. In the section 6.5, we will analyze the monopole strength distribution of ^{6}He. In the section 6.6, then we will analyze the dipole strength distribution from 0^+ ground state to the 1^- continuum state. Finally in the section 6.7, we will discuss octupole response of the system and finally we will draw some conclusions.

6.2 Pairing strength of different multipolarities

Theoretical investigation of very weakly-bound nuclei sitting right on top of the drip lines, demands proper consideration of nucleon-nucleon pairing interaction. An attractive pairing contact delta interaction has been used, $-G\delta(\vec{r}_1 - \vec{r}_2)$ for simplicity, because we can reach the goal with only one parameter adjustment. For ground state it is pretty much clear that, the pairing strength, G, is adjusted in order to get the correct ground state energy. But for higher multi-polarities i.e. J= 1^-, 2^+ and 3^- we do not have a clear-cut strategy to determine the exact value of pairing strength. For each value of J we tried different sets of values of G. From Fig-6.1, the upper limit of pairing strength can be found for several values of J, along with the number of states (red). Notice that different multipolarities give rise to different concentrations of strength as seen by comparing the densities of the various columns. Notice also that the continua are, at the eyes, quite dense, a condition that is necessary to reproduce minute features with the necessary accuracy.

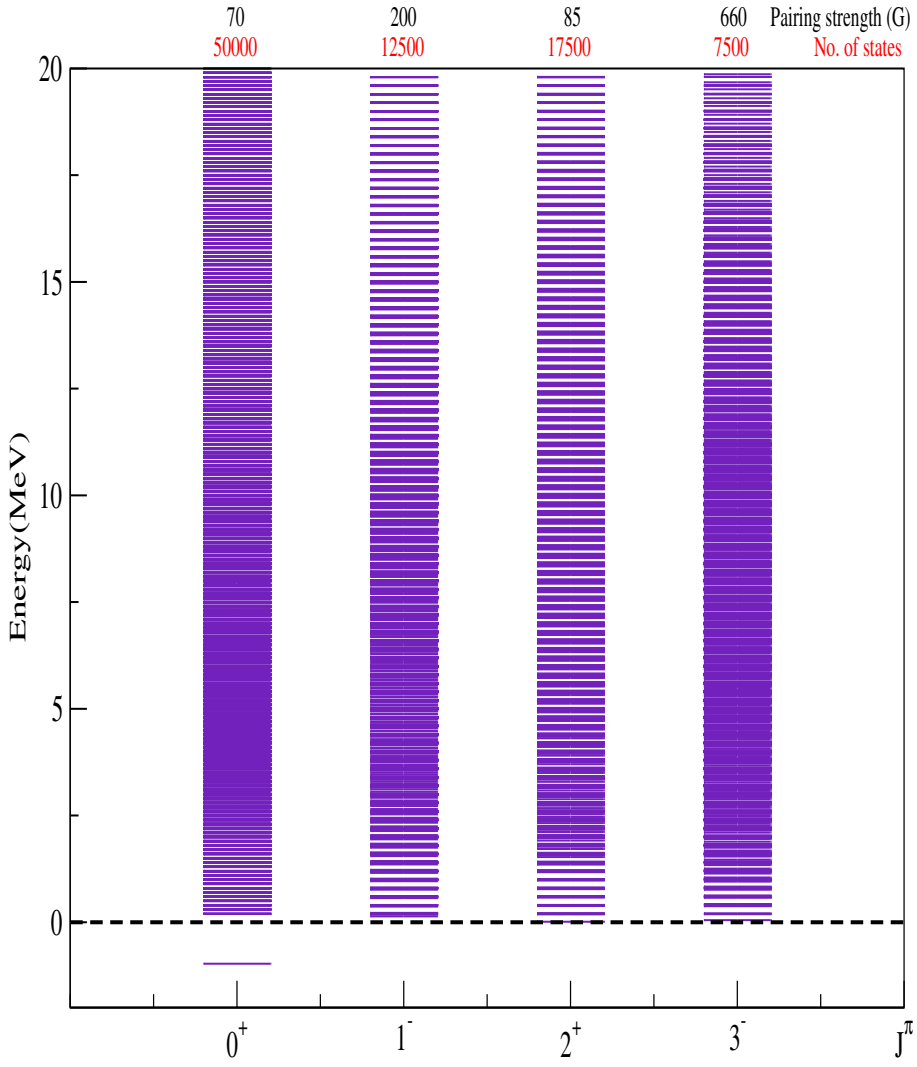

Figure 6.1: Eigenspectrum of the interacting two-particle case for $J^\pi = 0^+$, 1^-, 2^+ and 3^- for different number of states. The coefficient of the $\delta-$contact matrix, G, has also been shown for different J.

6.3 Electric transitions to continuum- Mathematical set up

The electric transition probability between ground state $\psi(j_1^{'}, j_2^{'}, J^{'}, M^{'})$ and continuum states $\psi(j_1, j_2, J, M)$ is given by

$$\begin{aligned}
&\langle\psi(j_1^{'}, j_2^{'}, J^{'}, M^{'})|\hat{O}_p|\psi(j_1, j_2, J, M)\rangle = \\
&\sum_{S',L'}\sqrt{(2S'+1)(2L'+1)(2j_1^{'}+1)(2j_2^{'}+1)}\begin{Bmatrix} 1/2 & \ell_1^{'} & j_1^{'} \\ 1/2 & \ell_2^{'} & j_2^{'} \\ S^{'} & L^{'} & J^{'}\end{Bmatrix} \\
&\sum_{S,L}\sqrt{(2S+1)(2L+1)(2j_1+1)(2j_2+1)}\begin{Bmatrix} 1/2 & \ell_1 & j_1 \\ 1/2 & \ell_2 & j_2 \\ S & L & J\end{Bmatrix} \\
&\Bigg([\langle R^{+}_{\ell_1^{'}\ell_2^{'}}(r_1r_2)\Upsilon^{+}_{L^{'}M^{'}}(\Omega_1\Omega_2)|\hat{O}_p|R^{+}_{\ell_1\ell_2}(r_1r_2)\Upsilon^{+}_{LM}(\Omega_1\Omega_2)\rangle] \\
&+[\langle R^{-}_{\ell_1^{'}\ell_2^{'}}(r_1r_2)\Upsilon^{-}_{L^{'}M^{'}}(\Omega_1\Omega_2)|\hat{O}_p|R^{-}_{\ell_1\ell_2}(r_1r_2)\Upsilon^{-}_{LM}(\Omega_1\Omega_2)\rangle]\Bigg)
\end{aligned} \tag{6.1}$$

where $\hat{O}_p$ is one body operator and given by

$$\hat{O}_p = e^{(\lambda)}_{eff}\Big(r_1Y_{\lambda\mu}(\hat{r}_1) + r_2Y_{\lambda\mu}(\hat{r}_2)\Big) \tag{6.2}$$

with $\lambda = 1$ for dipole, $\lambda = 2$ for quadrupole and $\lambda = 3$ for octupole. $e^{(\lambda)}_{eff}$ is the the effective charge, tabulated in Table- (6.1) for different multipolarities and is given by

$$e^{(\lambda)}_{eff} = \frac{A_1^{\lambda}Z_2 + (-1)^{\lambda}A_z^{\lambda}Z_1}{A^{\lambda}} \tag{6.3}$$

Using Eq.(6.2), Eq.(6.1) can be rewritten as

Table 6.1: Effective charge for different multipolarities.

λ	$(e_{eff}^{(\lambda)})^2$
0 (Monopole)	4
1 (Dipole)	4/25
2 (Quadrupole)	4/625
3 (Octupole)	4/15625

$$
\begin{aligned}
&\langle\psi(j_1^{'}, j_2^{'}, J^{'}, M^{'})|\hat{O}_p|\psi(j_1, j_2, J, M)\rangle = \\
&\sum_{S^{'},L^{'}} \sqrt{(2S^{'}+1)(2L^{'}+1)(2j_1^{'}+1)(2j_2^{'}+1)} \begin{Bmatrix} 1/2 & \ell_1^{'} & j_1^{'} \\ 1/2 & \ell_2^{'} & j_2^{'} \\ S^{'} & L^{'} & J^{'} \end{Bmatrix} \\
&\sum_{S,L} \sqrt{(2S+1)(2L+1)(2j_1+1)(2j_2+1)} \begin{Bmatrix} 1/2 & \ell_1 & j_1 \\ 1/2 & \ell_2 & j_2 \\ S & L & J \end{Bmatrix} \\
&2\Big(\iint R^{+}_{\ell_1^{'}\ell_2^{'}}(r_1 r_2) r_1 R^{+}_{\ell_1\ell_2}(r_1 r_2) r_1^2 dr_1 r_2^2 dr_2 \\
&\langle \Upsilon^{+}_{L^{'}M^{'}}(\Omega_1\Omega_2)|Y_{\lambda\mu}(\Omega_1)|\Upsilon^{+}_{LM}(\Omega_1\Omega_2)\rangle \\
&+ \iint R^{-}_{\ell_1^{'}\ell_2^{'}}(r_1 r_2) r_1 R^{-}_{\ell_1\ell_2}(r_1 r_2) r_1^2 dr_1 r_2^2 dr_2 \\
&\langle \Upsilon^{-}_{L^{'}M^{'}}(\Omega_1\Omega_2)|Y_{\lambda\mu}(\Omega_1)|\Upsilon^{-}_{LM}(\Omega_1\Omega_2)\rangle \Big)
\end{aligned} \tag{6.4}
$$

Also $R^{\pm}_{\ell_1^{'}\ell_2^{'}}(r_1 r_2)$ and $\Upsilon^{\pm}_{L^{'}M^{'}}$ are given by

$$
\begin{aligned}
R^{\pm}_{\ell_1\ell_2}(r_1 r_2) = \quad & \frac{1}{r_1 r_2 \sqrt{2}} \\
& [R_{n_1\ell_1}(r_1) R_{n_2\ell_2}(r_2) \pm R_{n_2\ell_2}(r_1) R_{n_1\ell_1}(r_2)]
\end{aligned} \tag{6.5}
$$

$$
\begin{aligned}
\Upsilon^{\pm}_{LM} = \quad & \frac{1}{\sqrt{2}} \sum \langle \ell_1 m_1 \ell_2 m_2 | \ell_1 \ell_2 L M \rangle \\
& [Y_{\ell_1 m_1}(\Omega_1) Y \ell_2 m_2(\Omega_2) \pm Y_{\ell_2 m_2}(\Omega_1) Y_{\ell_1 m_1}(\Omega_2)]
\end{aligned} \tag{6.6}
$$

Using Eq.(6.5) and Eq. (6.6), Eq.(6.4) gives us the matrix elements of different multipolarities. Eq.(6.4) consists of two parts i.e. evaluation of radial parts and angular parts. For evaluation of radial integrals, we need the corresponding two-particle wave function, whereas for the angular part by making use of Eq.(6.6), we will simplify the angular part and for different multipolarities these can be calculated easily and are tabulated in Tables – (6.2, 6.3 and 6.4) below.

6.4 Monopole strength distribution

Electric monopole transition strengths reflect the off-diagonal matrix elements of the E0 operator. The E0 operator [123] can be expressed in terms of single-nucleon degrees of freedom as

$$\hat{T}(E0) = \sum_k e_k r_k^2 \tag{6.7}$$

The E0 transition rate, $1/\tau(E0) = \rho_{fi}^2$, is defined by

$$\rho_{fi}^2 = \left| \frac{\langle f | \sum_k e_k r_k^2 | i \rangle}{eR^2} \right|^2 \tag{6.8}$$

where, e is the unit of electrical charge, and R is the nuclear radius,$R \backsimeq 1.2A^{1/3}$ fm. These calculations also leads us to study the role of various configurations in the total monopole strength. After constructing a basis of the largest size(N= 100) made up of five parts, namely $[(s_{1/2})^2]^0$, $[(p_{1/2})^2]^0$, $[(p_{3/2})^2]^0$, $[(d_{3/2})^2]^0$ and $[(d_{5/2})^2]^0$, we diagonalize the pairing matrix and obtain eigenvalues, only one bound and remaing all are unbound, and the corresponding eigenvectors. Fig. (6.2), shows along with well established ground state, we have continuum 0^+ states with different contributions from

Table 6.2: Coefficients for symmetric angular part for 1^-.

Configuration	l1p	l2p	l1	l2	μ	Coefficient
$s1s1 - s1p1$	0	0	0	1	1 0 -1	0 $1/(2\sqrt{\pi})$ 0
$s1s1 - s1p3$	0	0	0	1	1 0 -1	0 $1/(2\sqrt{\pi})$ 0
$p1p1 - s1p1$	1	1	0	1	1 0 -1	0 $-1/(2\sqrt{3\pi})$ 0
$p1p1 - p1d3$	1	1	1	2	1 0 -1	0 $1/5\sqrt{2/3\pi} + 1/10\sqrt{6/\pi}$ 0
$p3p3 - s1p3$	1	1	0	1	1 0 -1	0 $-1/(2\sqrt{3\pi})$ 0
$p3p3 - p3d3$	1	1	1	2	1 0 -1	0 $1/5\sqrt{2/3\pi} + 1/10\sqrt{6/\pi}$ 0
$p3p3 - p3d5$	1	1	1	2	1 0 -1	0 $1/5\sqrt{2/3\pi} + 1/10\sqrt{6/\pi}$ 0
$d3d3 - p1d3$	2	2	1	2	1 0 -1	0 $-1/\sqrt{10\pi}$ 0
$d3d3 - p3d3$	2	2	1	2	1 0 -1	0 $-1/\sqrt{10\pi}$ 0
$d5d5 - p3d5$	2	2	1	2	1 0 -1	0 $-1/\sqrt{10\pi}$ 0

Table 6.3: Coefficients for symmetric angular part for 2^+.

Configuration	l1p	l2p	l1	l2	μ	Coefficient
$s1s1 - s1d3$	0	0	0	2	1 0 −1	0 $1/(2\sqrt{\pi})$ 0
$s1s1 - s1d5$	0	0	0	2	1 0 −1	0 $1/(2\sqrt{\pi})$ 0
$p1p1 - p1p3$	1	1	1	1	1 0 −1	0 $-\sqrt{2/(5\pi)}$ 0
$p3p3 - p1p3$	1	1	1	1	1 0 −1	0 $-\sqrt{2/(5\pi)}$ 0
$p3p3 - p3p3$	1	1	1	1	1 0 −1	0 $-\sqrt{2/(5\pi)}$ 0
$d3d3 - s1d3$	2	2	0	2	1 0 −1	0 $1/(2\sqrt{5\pi})$ 0
$d3d3 - d3d3$	2	2	2	2	1 0 −1	0 $-\sqrt{2/(7\pi)}$ 0
$d3d3 - d3d5$	2	2	2	2	1 0 −1	0 $-\sqrt{2/(7\pi)}$ 0
$d5d5 - s1d5$	2	2	0	2	1 0 −1	0 $1/(2\sqrt{5\pi})$ 0
$d5d5 - d3d5$	2	2	2	2	1 0 −1	0 $-\sqrt{2/(7\pi)}$ 0
$d5d5 - d5d5$	2	2	2	2	1 0 −1	0 $-\sqrt{2/(7\pi)}$ 0

Table 6.4: Coefficients for symmetric angular part for 3^-.

Configuration	l1p	l2p	l1	l2	μ	Coefficient
$p1p1 - p1d5$	1	1	1	2	1 0 -1	0 $-1/2\sqrt{3/(7\pi)}$ 0
$p3p3 - p3d3$	1	1	1	2	1 0 -1	0 $-1/2\sqrt{3/(7\pi)}$ 0
$p3p3 - p3d5$	1	1	1	2	1 0 -1	0 $-1/2\sqrt{3/(7\pi)}$ 0
$d3d3 - p3d3$	2	2	1	2	1 0 -1	0 $3/(2\sqrt{35\pi})$ 0
$d5d5 - p1d5$	2	2	1	2	1 0 -1	0 $3/(2\sqrt{35\pi})$ 0
$d5d5 - p3d5$	2	2	1	2	1 0 -1	0 $3/(2\sqrt{35\pi})$ 0

five different possible configurations for different basis dimensions. In order to reduce computation time, we have performed a set of calculations for monopole transitions from ground state 0^+ for basis size N= 100 to the continuum 0^+ for basis size N= 50. From Fig. (6.3), it is clear that there are only five possible transitions from 0^+ ground state components to continuum 0^+ states components. With all these necessary ingredients i.e. ground state and continuum 0^+ states, the monopole strength distribution has been studied. The upper panel of Fig. (6.4), shows the total monopole transition strength of ^{6}He and lower panel of Fig. (6.4), shows the contribution of various possible transitions on logarithmic scale. From lower panel Fig. (6.4), it is clear that the transition $[(p_{3/2})^2]^0$(g.s.)$\rightarrow$ $[(p_{3/2})^2]^0$(continuum), is dominant in the monopole transition strength, where as the transition $[(d_{3/2})^2]^0$(g.s.)$\rightarrow$ $[(d_{3/2})^2]^0$(continuum) is the least significant in total monopole transition strength. From this, one can also see that transition $[(s_{1/2})^2]^0$(g.s.)$\rightarrow$ $[(s_{1/2})^2]^0$(continuum) has significant contribution to the total strength, which justifies the inclusion of sd- shell in calculations. The total integrated monopole strength amounts to about $2682.97 fm^4$. This value can be compared with the non energy weighted sum rule calculations for monopole strength $2800 fm^4$ obtained in Ref. [124], giving a very good agreement.

6.5 Dipole strength distribution

While most theoretical studies have focused on dipole strength [76, 125, 126], our includes many more multipolarities. In order to compare our approach with others, we have also performed a set of calculations for dipole response from ground state to all components of 1^- state. After constructing a ba-

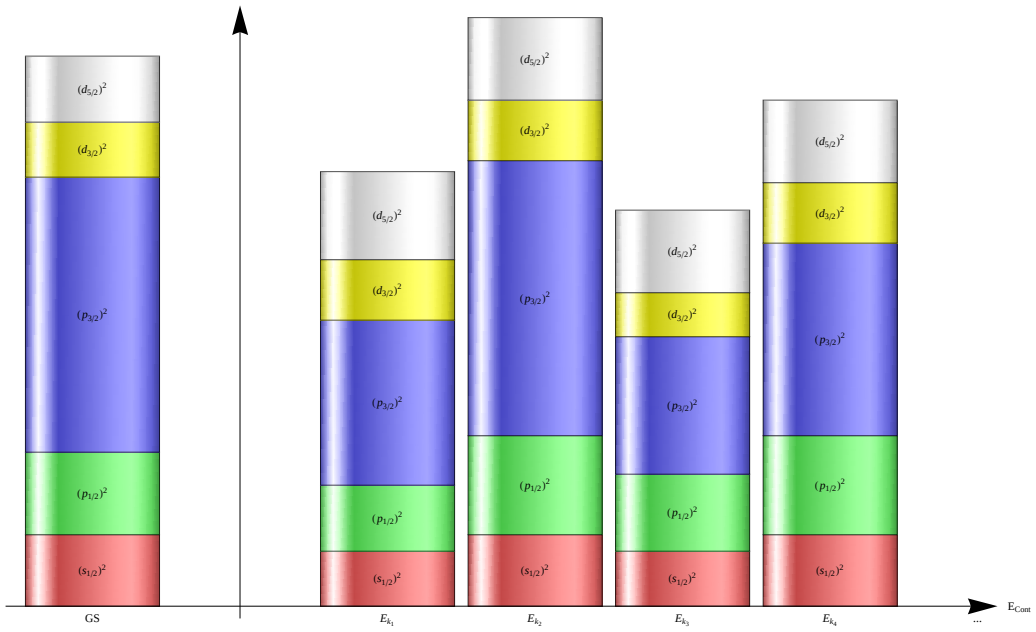

Figure 6.2: Schematic representation of groundstate (0^+) and continuum 0^+ states with different contributions from five different possible configurations.

sis of the dimensions N= 50, made up of five parts, namely $[s_{1/2} \times p_{1/2}]^1$, $[s_{1/2} \times p_{3/2}]^1$, $[p_{1/2} \times d_{3/2}]^1$, $[p_{3/2} \times d_{3/2}]^1$ and $[p_{3/2} \times d_{5/2}]^1$, we diagonalize the pairing matrix and obtain eigenvalues, that are all unbound, and the corresponding eigenvectors. We did calculations for three different values of pairing strength G i.e. 0, 100 and 200(upper limit to get all states unbound). From Fig. (6.5), it is clear that there are total 10 different transitions are possible from initial 0^+ ground state to the final 1^- state of ^{6}He. We have investigated the detailed structure of $E1$ (dipole) strength distribution from two perspectives, one is to fix the pairing strength and second is to study the role of different configurations. Fig. (6.6), shows the total dipole transition strength of ^{6}He with different values of G and Table- (6.5) tabulates the total B(E1) strength in e^2fm^2 with pairing strength G. As it should, it remains practically constant. The shape of our dipole response function more or less

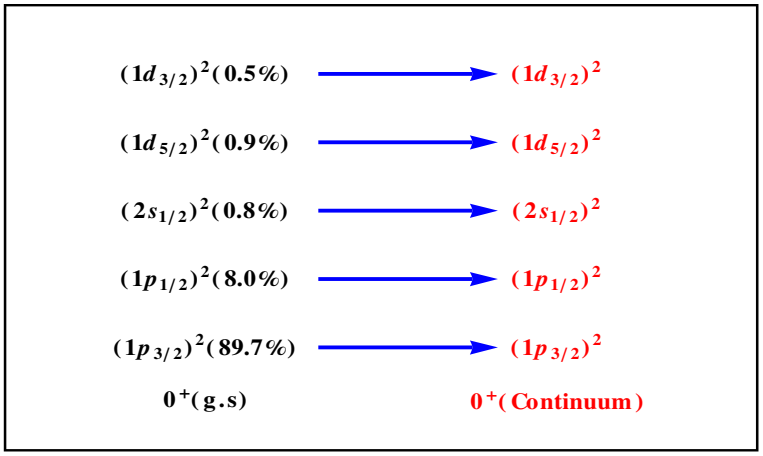

Figure 6.3: Total number of possible monopole transitions from ground state 0^+ to the final continuum 0^+ states with different contributions from five different possible configurations for ^{6}He.

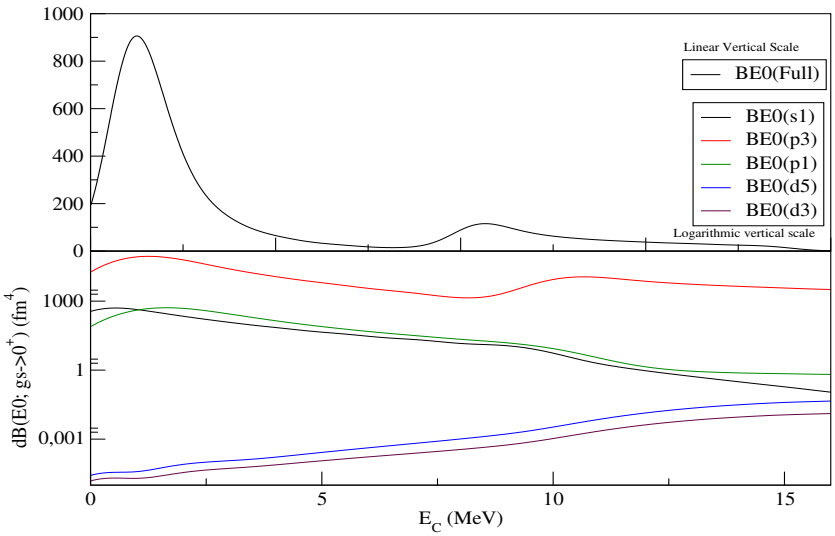

Figure 6.4: (Upper panel) Total monopole $E0$ transition strength distribution (on linear vertical scale) from ground state 0^+ to the final state 0^+ for ^{6}He. (Lower panel) Component monopole $E0$ transition strength distribution (on logarithmic vertical scale) from ground state 0^+ to the final state 0^+ for ^{6}He.

Table 6.5: Total B(E1) with pairing strength.

G	Total B(E1) e^2fm^2
0	1.8747
100	1.8736
200	1.8378

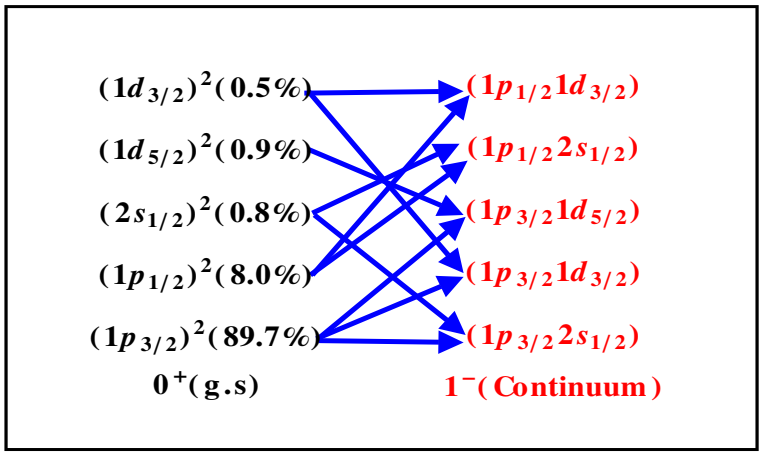

Figure 6.5: Total number of possible dipole transitions from ground state 0^+ to the final state 1^- with different contributions from five different possible configurations for ^{6}He.

matches with the previous calculations [127, 76, 125, 126]. As a result of the smoothing procedure, the curves in Fig. (6.6) show a few minor wiggles, that are not to be attributed to the resonances, but must be considered as an artifact. It is clear though that there is an accumulation of strength at energies of $2-10$ MeV and possibly a shallow maximum around $3-5$ MeV. Also it is clear from these calculations that the transition from $[p_{3/2} \times p_{3/2}]^0$ $\rightarrow$ $[p_{3/2} \times d_{5/2}]^1$ plays the significant role in total dipole transition strength, whereas all other remaining nine transitions are less significant.

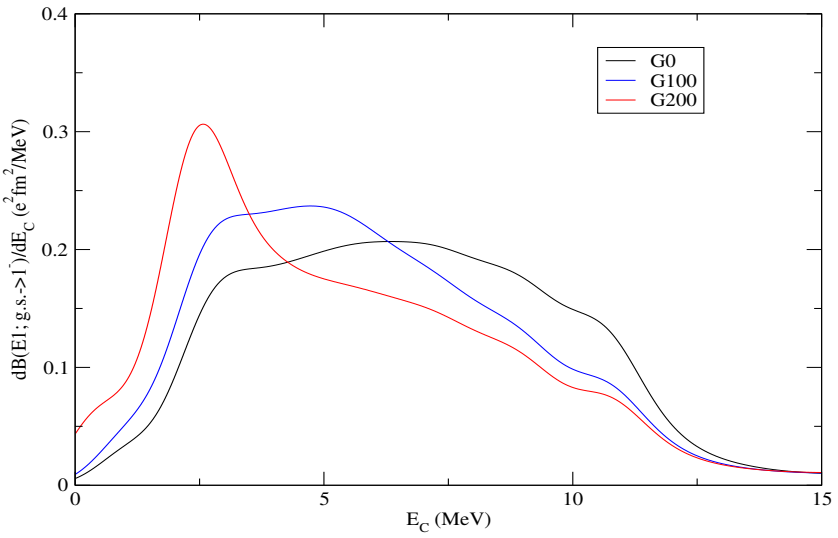

Figure 6.6: Dipole $E1$ transition strength distribution from ground state 0^+ to the final state 1^- for ^{6}He for a few values of the pairing strength.

6.6 Quadrupole strength distribution

Due to limitation of computation time, quadrupole response of ^{6}He has been studied in reduced model space. After constructing a basis of the dimensions $N = 100$ made up of two parts, namely $[p_{3/2} \times p_{3/2}]^{(2)}$ and $[p_{3/2} \times p_{1/2}]^{(2)}$, we diagonalize the pairing matrix and obtain eigenvalues, that are all unbound, and the corresponding eigenvectors. Notice that in Ref. [74] the response function is given only for the dipole mode, but the cross-section of Fig. 1(b), although not always directly comparable with a response function, has a quadrupole component that is very similar in shape to our results. In Fig. 11 of Ref. [79] the quadrupole inelastic strength function is shown, in good agreement with our results. We compute the B(E2) values (Fig. 6.7) to the continuum eigenstates and adjust also in this case the strength of the pairing matrix ($G_2 = 475.0$) to get the energy centroid of the first peak at about the right position ($E = 0.76$ MeV, ~ 0.2 MeV). The width is

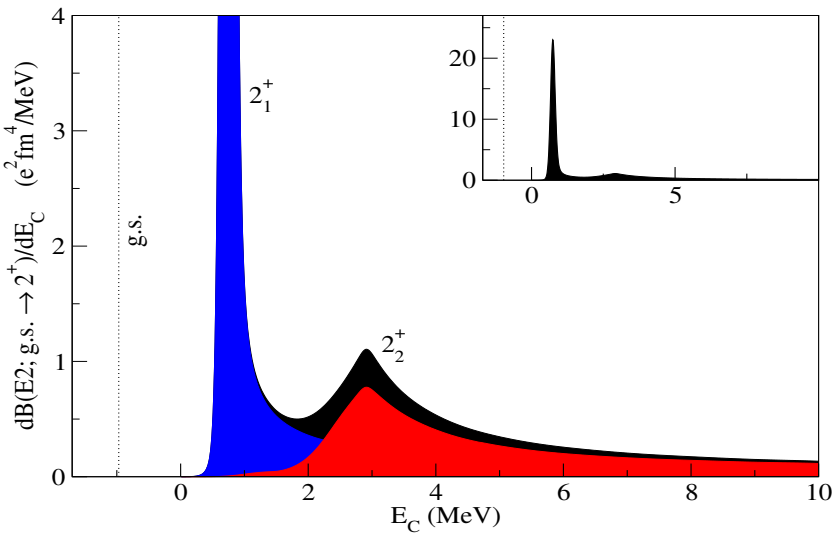

Figure 6.7: Quadrupole strength distribution with respect to the break up threshold. The total strength (black) is split into the contribution of the $(p_{3/2})^2$ and $(p_{3/2}p_{1/2})$ components, in blue and red respectively. The insert shows the full curve for the total strength.

a bit larger then the experimental value. We also obtain a second peak at about $E = 2.91$ MeV with an asymmetric width at half maximum of ~ 1.8 MeV. While the first peak is mainly due to $(p_3/2)^2$ components, the second peak is clearly identified as arising mainly from $(p_{3/2}p_{1/2})$ components. Measuring energies from the g.s., the second peak is found at about 3.88 MeV. A noteworthy feature of this peak is that it is found at an energy higher than the corresponding unperturbed two-particle state, despite the attractive nature of pairing: this is a consequence of mixing and of the asymmetric long tail in energy of the $p_{1/2}$ resonance in ^{5}He. The total integrated strength amounts to about $8.8e^2fm^4$. This value can be compared with the value of $9.7471e^2fm^4$ obtained in Ref. [127]. To the best of our knowledge Fig. 6 of that work is the only published theoretical prediction for $E2$ strength distribution in ^{6}He, and we essentially confirm that result. As mentioned

in the introduction, there is one model-dependent experimental extraction of the integrated quadrupole strength to the narrow 2^+ state that relies on a particular form of transition density, namely in Ref. [42] the value $(3.2 \pm 0.6)e^2fm^4$ is reported. Since the paper does not specify the range of integration in energy, we have integrated our results around the peak, taking into account the region of full width at half maximum and obtaining about $3.7 \pm 0.9e^2fm^4$, where the error estimate has been obtained considering the uncertainties in the energy centroid and width. Korennov and Descouvemont [80] obtain a smaller value of $2.89e^2fm^4$, but both are compatible with the experimental value.

6.7 Octupole strength distribution

In order to complete the studies, we have also investigated the detailed structure of $E3$ (Octupole) strength distribution of the system. After constructing a basis of the dimensions N= 50, made up of three parts, namely $[p_{1/2} \times d_{5/2}]^3$, $[p_{3/2} \times d_{3/2}]^3$ and $[p_{3/2} \times d_{5/2}]^3$, we diagonalize the pairing matrix and obtain eigenvalues, that are all unbound, and the corresponding eigenvectors. We did calculations for four different values of pairing strength G_3 i.e. 0, 250, 500 and 660(upper limit to get all states unbound). From Fig. (6.8), it is clear that there is a total of 6 different transitions from initial 0^+ ground state to the final continuum 3^- state of ^{6}He. Although we cannot integrate to find the total strength under curve, because we are not sure about having reached the maximum within the energy range investigated. Ideally, one should use a larger energy cut and maybe a smaller density of states. But in order to complete the studies, Table- (6.6) tabulates the total B(E3) strength in e^2fm^6 with pairing strength G. Fig. (6.9), shows the total dipole

Table 6.6: Total B(E3) with pairing strength G.

G	Total B(E3) e^2fm^6
0	91.2076
250	91.1592
500	91.0861
660	90.8239

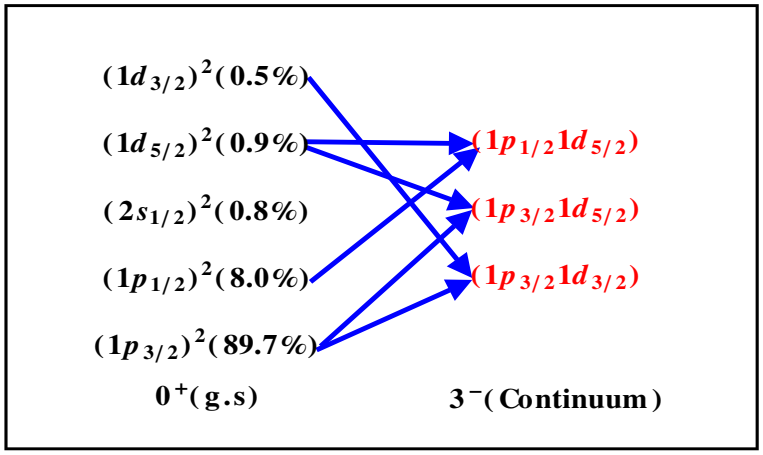

Figure 6.8: Schematic representation depicting all of the possible octupole transitions from ground state 0^+ emerging from five different configurations to the final state 3^- emerging from three different configurations for ^{6}He.

transition strength of ^{6}He with different values of G. The shape of our octupole response function shows two large structures around 1 MeV and 10 MeV respectively. Also it is clear from these calculations that transitions from $[p_{3/2} \times p_{3/2}]^0 \rightarrow [p_{3/2} \times d_{3/2}]^3$ and $[p_{3/2} \times p_{3/2}]^0 \rightarrow [p_{3/2} \times d_{5/2}]^3$ plays the significant role in total octupole transition strength approximately $\sim 59\%$ and $\sim 41\%$ respectively, where as all other remaining four transitions are comparatively less significant.

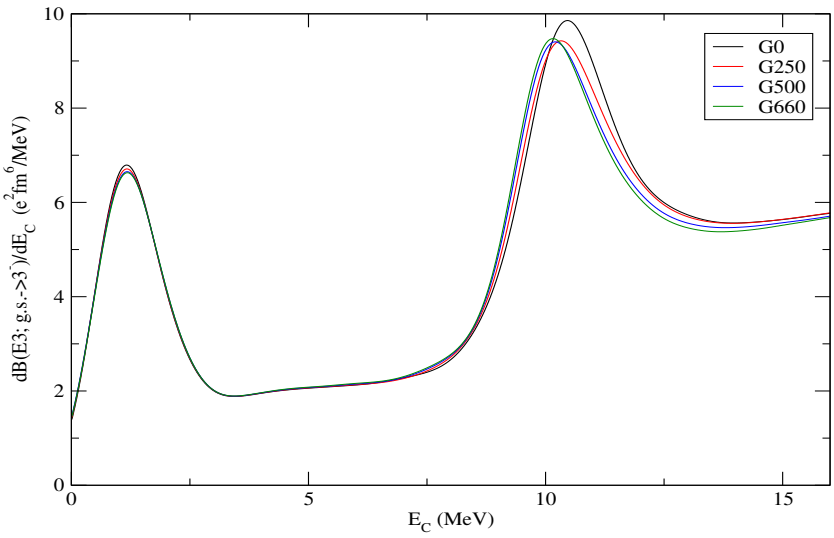

Figure 6.9: Octupole $E3$ transition strength distribution from ground state 0^+ to the final state 3^- for ^{6}He.

6.8 Conclusions

We analyzed the $E0, E1, E2$, and $E3$ response of ^{6}He, along with the role of various configurations in these electric transitions. The quadrupole response ($0^+ \rightarrow 2^+$ in reduced model space) for ^{6}He leads to finding the two resonances, the narrow low-lying 2^+ and a broader 2^+ at 2.9 MeV above threshold with a width of about 1.8 MeV. Whereas for the other multipolarities the total strength distribution has been reported along comparison with previous studies. Also the dominant transitions in each case have been discussed.

Chapter 7

Summary and future prespectives

7.1 Summary

In this thesis we have presented a simple nuclear structure model for ground and continuum states of Borromean nuclei and its application to ^{6}He that has been developed during three years of study and work in Padova.

We attacked this problem in very simple fashion, by keeping in mind the treatment of continuum as the one of the challenging issue at drip lines. We start from the true continuum, by coupling two copies of single particle continuum wave functions of the unbound subsystem.

The themes covered in the present thesis are: a detailed simple three body structure model formulation and procedure, the recipe to deal with continuum of the subsystem of Borromean nuclei, pairing interaction in continuum, two neutron density and finally electromagnetic response of the ^{6}He.

This study is quite challenging from the computational point of view, in particular for what concerns the handling of large data sets and the development of a series of codes discussed in detail in chapter-3. The whole methodology and results discussed in this thesis, in our opinion, are, interesting for the

nuclear physics community.

7.2 Future prespectives

In near future along with these studies, it is interesting to look at following points:

1. **Density dependent Pairing Interactions**
   More tests and calculations are needed to assess whether the earlier predictions with simple pairing contact-delta interaction for ^{6}He are modified by different choice of pairing interaction (density dependent) and energy cuts. Inclusion of recoil correction for dipole calculations can also be done.

2. **Test simple structure model for other Borromean candidates**
   In order to check our simple structure model applicability, it is worth to run the calculations for well known Borromean nuclei such as ^{11}Li and ^{14}Be.

3. **Magnetic transitions**
   Magnetic transitions $M1$ are feasible in this model space and are also interesting to calculate them along with electric transitions.

Appendices

Appendix A

Appendix

A.1 Procedure

The procedure adopted for these calculations is explained in Fig. (A.1) with the help of a flow chart diagram. It is divided in blocks that correspond to the various codes used. In each block yellow background indicates input lines where data must be passed to the code. Several types of inputs are required: most of them are integers or real number (mostly in convenient nuclear units) that must be set case-by-case, others are strings of text. Most input data are read in the input file.

A.1.1 Block 1

Block 1 calculates the *spd*−continuum single-particle states ($E_C > 0$) of ^{5}He with Woods-Saxon potential + spin-orbit potential [97], with energies from 0.1 to 10.0 MeV on a radial grid that goes from 0.1 to 100.0 fm (notice that this amount to 2.2 Mb of data for each component). The first two lines of input file for this block, loads nuclide information (number of protons and mass number for core and cluster), followed by Woods-Saxon poten-

tial and spin-orbit potential parameters used to generate the single-particle wave functions and then quantum numbers (spins, orbital and total angular momenta) are read, these depend on the single particle state under investigation. This block calculates eigenstates and eigenvalues of 3D Schroedinger equation with Woods-Saxon potential+spin-orbit potential for given nuclide for continuum states. A script file called looper.sh is used for external looping over energy of continuum. Single-particle wave functions are collected in a formatted table after reading the input file. These wavefunction files can be set up with two columns, one for the radial variable in fm and one for the calculated wavefunction. The spacing in the radial variable must necessarily be constant. With the help of looper.sh we can generate output files with name string *cont_ energy_ ii.dat*, where *ii* refers to energy of state. All calculated single-particle wave functions are stored in respective directories properly named as spd.

A.1.2 Block 2

By using the midpoint method (for explanation see next chapter) as a discretization recipe, the wave functions are normalized to a Dirac delta in energy with an energy spacing of $2.0, 1.0, 0.5, 0.2$, and 0.1 MeV corresponding to block basis dimensions of $N = 5, 10, 20, 50$, and 100 respectively. The various parameters used in these calculations are tabulated in Table-A.1. The input file for this block loads the step between continuum states, total number of states to be included in model space (for this case it is 5 see last column of Table-A.1) and strings of output file names. Two-particle states are constructed with proper couplings to J= $0^+, 1^-, 2^+, 3^-$. This block evaluates integral of contact delta pairing interaction between two sets of two single-particle continuum orbitals. The output is saved in matrix blocks. For

Table A.1: Various parameters used for full model space calculations (i.e. spd- shell in picture).

Basis size (N)	Energy interval (ΔE)	Energy step (istp)	No. of states (nstat=N^2)	lda (=5*nstat)
5	2	20	25	125
10	1	10	100	500
20	0.5	5	400	2000
50	0.2	2	2500	12500
100	0.1	1	10000	50000

ground state J= 0^+ and J= 1^-, it amounts to calculation of 15 matrix blocks (approximately $\sim$ 9 Gb of data) , for J= 2^+ state it amounts to calculation of 28 matrix blocks, which is a hard computational task and for J= 3^-, it amounts to calculation of 6 matrix blocks.

A.1.3 Block 3

It simply reads the matrix blocks evaluated in block-2 and multiply them with appropriate coefficients which are evaluated in a separate Mathematica notebook and calculates the matrix elements of pairing matrix. The input file of this block loads all the appropriate coefficients and for all these states the coefficients of matrix elements are calculated for upper diagonal part of the matrix only due to symmetry. The output pairing matrix is huge data set file ($\sim$ 21 Gb of data for the largest case in ground state). Pairing matrix is generated for all different basis dimensions N = $5, 10, 20, 50$, and 100 respectively.

A.1.4 Block 4

It simply diagonalizes the pairing matrix with standard routines to give eigenvalues and eigenvectors. The actual pairing interaction g is obtained by cor-

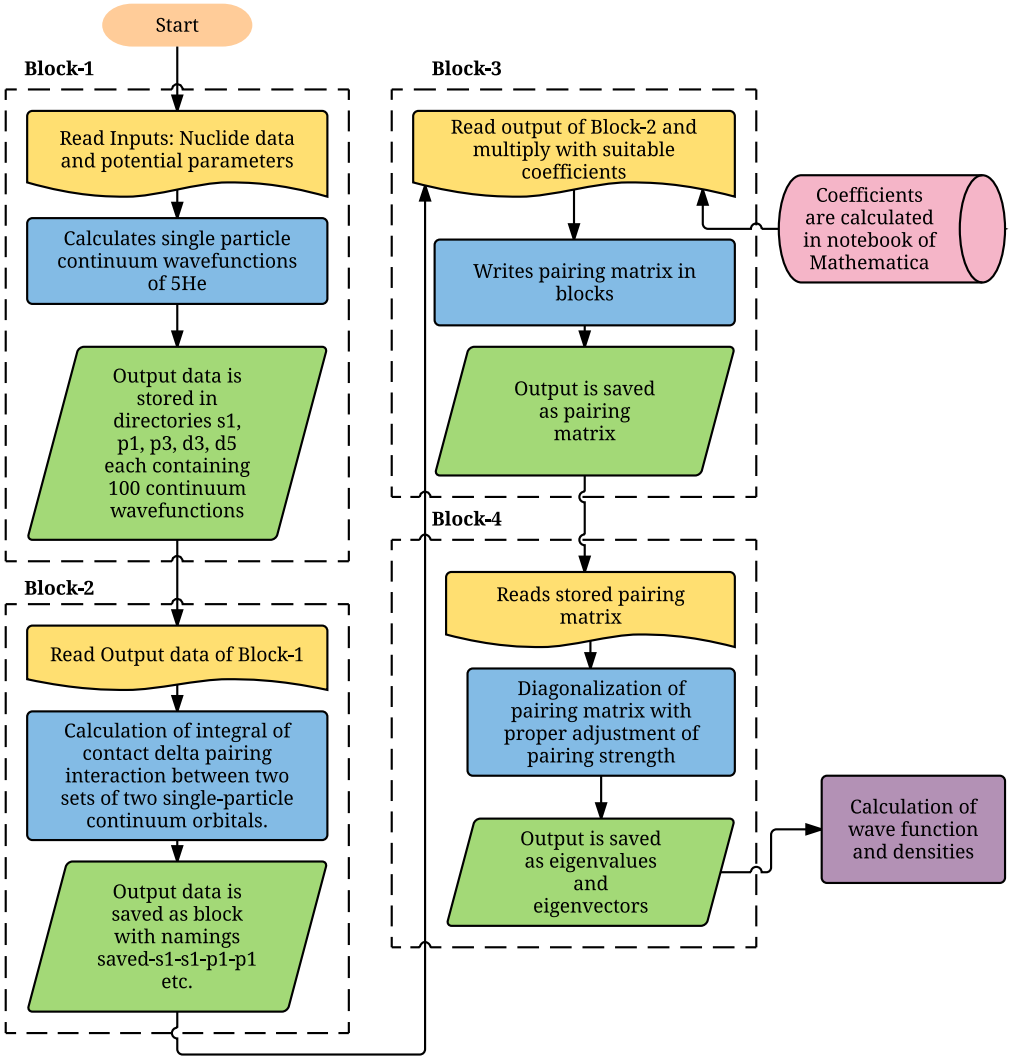

Figure A.1: Flow chart diagram of procedure followed with series of codes used. Blocks are indicated with dashed black boxes. Inside each block data reading is indicated as light yellow cards, algorithms are indicated as blue rectangles and outputs in green. The pink cylinder indicates feeding of certain coefficients from outside, while the violet box indicates quantities that are obtained through additional calculations.

recting with a factor that depends on the aforementioned spacing between

energy states ΔE and is given by a relation

$$G = g(\Delta E)^2 \tag{A.1}$$

The coefficient of the $\delta-$contact matrix, G for $J = 0^+$ case, has been adjusted to reproduce the correct ground state energy each time. The biggest adopted basis size gives a fairly dense continuum in the region of interest. The output of block 4 is further used for calculation of ground state wavefunction, transition probabilities and two particle densities. For higher multipolarities i.e. J= 1^-, J= 2^+, and J=3^-, we don't have a clear way to set the exact value of pairing strength, although for the J= 2^+ case, we can use the narrow resonance to set the value of G_2. Nevertheless we can identify a procedure, by which we can establish a minimum value (that is zero pairing) and a maximum value. For each value of J we tried different sets of values of G, we fixed the upper limit of G for each case as the last value that gives only unbound states. A slightly stronger pairing would give a bound state in a $J \neq 0$ channel, that is not experimentally observed.

Bibliography

[1] R. Bennett, P. Van Duppen, H. Geissel, K. Heyde, B. Jonson, O. Kester, G.E. Körner, W. Mittig, A.C. Mueller, G. Münzenberg, H.L. Ravn, K. Riisager, G. Schrieder, A. Shotter, J.S. Vaagen, J. Vervier, NuPECC Report on & Radioactive Nuclear Beam Facilities, April 2000.

[2] I. Tanihata, H. Hamagaki, O. Hashimoto, Y. Shida, N. Yoshikawa, K. Sugimoto, O. Yamakawa, T. Kobayashi, and N. Takahashi, Phys. Rev. Lett. **55**, 2676 (1985).

[3] I. Tanihata et al., Phys. Lett. **B 160**, 380 (1985).

[4] T. Motobayashi, Nucl. Phys. **A 834**, 707 (2010).

[5] H. Sakurai, Nucl. Phys. **A 834**, 388C (2010).

[6] I. Augustin, Nucl. Inst. Methods Phys. Res. **B 261**, 1014 (2007).

[7] M. Thoennessen, Nucl. Phys. **A 834**, 688C (2010).

[8] S. Gales, Nucl. Phys. **A 834**, 717C (2010).

[9] E. Kugler, D. Fiander, B. Johnson, H. Haas, A. Przewloka, H. L. Ravn, D. J. Simon and K. Zimmer, Nucl. Inst. Methods Phys. Res. **B 70**, 41 (1992).

[10] G. M. Ter-Akopian, Yu. Ts. Oganessian, M. G. Itkis, G. G. Gulbekian, D. D.Bogdanov, A. S. Fomichev, M. S. Golovkov, A. M. Rodin, S. V. Stepantsov, R. Wolski, Nucl. Phys. **A 734**, 95 (2004).

[11] I. Tanihata, H. Savajols and R. Kanungo, Prog. Part. Nucl. Phys. **68**, 215 (2013).

[12] K. Hagino, I. Tanihata and H. Sagawa, arXiv:1208.1583 [nucl-th], (2012).

[13] P. G. Hansen and B. M. Sherill, Nucl. Phys. **A 693**, 133 (2001).

[14] I. Tanihata, Nucl. Phys. **A 654**, C235 (1999).

[15] B. Jonson, Nucl. Phys. **A 631**, 376 (1998).

[16] I. Tanihata, Neutron halo nuclei, J. Phys. **G 22**, 157 (1996).

[17] P. G. Hansen, A. S. Jensen and B. Jonson, Ann. Rev. Nucl. Part. Sci. **45**, 591 (1995).

[18] K. Riisager, Rev. Mod. Phys. **66**, 1105 (1994).

[19] P. G. Hansen and B. Jonson, Europhys. Lett **4** 409 (1987).

[20] B. Jonson and K. Riisager, Philos. Trans. Roy. Soc. London Ser. **A 356**, 2063 (1998).

[21] I. Tanihata et al., Phys. Lett. **B 206**, 592 (1985).

[22] T. Bjerge, K.J. Borgström, Nature **138**, 400 (1936).

[23] M. Fukuda et al., Phys. Lett. **B 268**, 339 (1991).

[24] D. Bazin et al., Phys. Rev. **C 57**, 2156 (1998).

[25] V. Guimaraes et al., Phys. Rev. **C 61**, 064609 (2000).

[26] D. Bazin et al., Phys. Rev. Lett. **74**, 3569 (1995).

[27] M.D. Cortina-Gil et al., Phys. Lett. **B 371**, 14 (1996).

[28] I. Tanihata et al., Phys. Lett. **B 287**, 307 (1992).

[29] T. Suzuki et al., Nucl. Phys. **A 658**, 313 (1999).

[30] M. Labiche et al., Phys. Rev. Lett. **86**, 600 (2001).

[31] J. S. Al-Khalili and J. A. Tostevin, Phys. Rev. Lett. **76**, 3903 (1996).

[32] M.V. Zhukov, B.V. Danilin, D.V. Fedorov, J.M. Bang, I.J. Thompson and J.S. Vaagen, Phys. Rep. **231**, 151 (1993).

[33] A. S. Jensen and K. Riisager, Phys. Lett. **B 480**, 39 (2000).

[34] T. Frederico, A. Delfino, Lauro Tomio, M.T. Yamashita, Progress in Particle and Nuclear Physics **67**, 939, (2012).

[35] C.A. Bertulani, Nuclear Physics in a Nutshell, Princeton University Press (2007).

[36] K. Tanaka et al., Phys. Rev. Lett. **104**, 062701 (2010).

[37] M. Matsuo, Phys. Rev. **C 73**, 044309 (2006).

[38] G.F. Bertsch, H. Esbensen, Ann. Phys. (N.Y.) **209**, 327 (1991).

[39] T. Otsuka, R. Fujimoto, Y. Utsuno, B. A. Brown, M. Honma and T. Mizusaki Phys. Rev. Lett. **87** 082502 (2001).

[40] T. Kobayashi et al., Phys. Rev. Lett. **60**, 2599 (1988).

[41] N. Fukuda et al., Phys. Rev. **C 70**, 054606 (2004).

[42] T. Aumann et al., Phys. Rev. **C 59**, 1252 (1999).

[43] T. Nakamura et al., Phys. Rev. Lett. **96**, 252502 (2006).

[44] M. A. Nagarajan, S. M. Lenzi, A. Vitturi, Eur. Phys. J. **A 24**, 63 (2005).

[45] B.V. Danilin, et al., Phys. Rev. **C 55**, 577 (1997).

[46] F. Brady, G. A. Needham, J. L. Romero, C. M. Castaneda, T.D. Ford, J. L. Ullmann, and M. L. Webb, Phys. Rev. Lett. **51**, 1320 (1983); F. Brady, G. A. Needham, J. L. Ullmann, C. M. Castaneda, T. D. Ford, N. S. P. King, J. L. Romero, M. L.Webb, V. R. Brown, and C. H. Poppe, J. Phys. **G 10**, 363 (1984).

[47] F. Ajzenberg-Selove, Nucl. Phys. **A 490**, 1 (1988).

[48] F. Ajzenberg-Selove, Nucl. Phys. **A 506**, 1 (1990).

[49] J. C. Roynette, M. Arditi, J. C. Jacmart, F. Mazloum, M. Riou and C. Ruhla, Nucl. Phys. **A95**, 545 (1967).

[50] F. P. Brady, Phys. Rev. C **16**, 31 (1977).

[51] K. Shoda, M. Torikoshi, O. Sasaki, S. Toyama, T. Kobayashi, A. Kagaya H. Tsubota, Phys. Rev. C **33**, 2179 (1986).

[52] J. Jänecke et al., Phys.Rev. C **54**, 1070 (1996).

[53] S. Nakayama et al., Phys. Rev. Lett. **85**, 262 (2000).

[54] S. Nakayama et al., Phys. Rev. Lett. **87**, 122502 (2001).

[55] T. Nakamura et al., Phys. Lett. **B 493**, 209 (2000).

[56] T. Nakamura, Eur. Phys. J. A **13** 33-37, (2002).

[57] H. Akimune et al., Phys.Rev. C **67**, 051302**(R)** (2003).

[58] X. Mougeot et al., Phys. Lett. B **718** (2012) 441-446.

[59] O. M. Povoroznyk, V. S. Vasilevsky, Ukr. J. Phys. **60**, 3, (2015).

[60] A. B. Migdal, Sov. J. Nucl. Phys. **16**, 238 (1973).

[61] S. Aoyama, S. Mukai, K. Kato and K. Ikeda, Prog. Theor. Phys. **93**, 99 (1995).

[62] A. Csótó, Phys. Rev. **C48**, 165 (1993).

[63] K. Arai, Y. Suzuki and R. G. Lovas, Phys. Rev. **C59**, 1432 (1999).

[64] N. Michel, W. Nazarewicz, M. Ploszajczak, K. Bennaceur, Phys. Rev. Lett., **89**, 042502 (2002).

[65] N. Michel, W. Nazarewicz, M. Ploszajczak, K. Bennaceur, Phys. Rev. C **67**, 054311 (2003).

[66] G. Hagen, M. Hjorth-Jensen, J.S. Vaagen, Phys. Rev. C **71**, 044314 (2005).

[67] N. Michel, W. Nazarewicz, M. Ploszajczak,Phys. Rev. C, **82**, 044315 (2010).

[68] A. Volya, V. Zelevinsky, Phys. Rev. Lett., **94**, 052501 (2005).

[69] T. Myo, K. Kato and K. Ikeda, Phys. Rev. **C76**, 054309 (2007).

[70] M. V. Zhukov, B. V. Danilin, D. V. Fedorov, J. M. Bang, I. J. Thompson and J. S. Vaagen, Phys. Rep. **231**, 151-199 (1993).

[71] S. C. Pieper, R. B. Wiringa, and J. Carlson, Phys. Rev. C **70**, 054325 (2004).

[72] P. Navrátil and W. E. Ormand, Phys. Rev. C **68**, 034305(2003).

[73] P. Navrátil, J. P. Vary, W. E. Ormand, and B. R. Barrett, Phys. Rev. Lett. 87, 172502 (2001).

[74] B. V. Danilin, T. Rogde, S. N. Ershov, H. Heiberg-Andersen, J. S. Vaagen, I. J. Thompson, and M. V. Zhukov, Phys. Rev. C 55, R577 (1997).

[75] P. Mei and P. Van Isacker, Ann.Phys.(N.Y.) **327**, 1162-1181 (2012).

[76] D. Mikami, W. Horiuchi, and Y. Suzuki, Phys.Rev.C **89**,064303(2014).

[77] K. Hagino and H. Sagawa, Phys.Rev. C **72**, 044321 (2005).

[78] C. Romero-Redondo, S. Quaglioni, P. Navrátil and G. Hupin, Phys.Rev.Lett. **113**, 032503 (2014).

[79] B. V. Danilin, I. J. Thompson, J. S. Vaagen, and M. V.Zhukov, Nucl. Phys. **A 632**, 383 (1998).

[80] S. Korennov and P. Descouvemont, Nucl. Phys. A740, 249(2004).

[81] A. Damman and P. Descouvemont, Phys. Rev. C 80, 044310(2009).

[82] L. Fortunato, R. Chatterjee, Jagjit Singh and A. Vitturi, Phys. Rev. C **90**, 064301 (2014).

[83] S. Baroni, P. Navrátil, S. Quaglioni, Phys. Rev. Lett. **110**, 022505 (2013).

[84] H. T. Fortune, Phys.Rev. C **89**, 014326 (2014).

[85] H. Esbensen, G.F. Bertsch and K. Hencken, Phys.Rev. C **56**, 3054-3062 (1997).

[86] B. V. Danilin, T. Rogde, S. N. Ershov, H. Heiberg-Andersen, J. S. Vaagen, I. J. Thompson, and M. V. Zhukov, Phys. Rev. **C 55**, R577 (1997).

[87] B. V. Danilin, I. J. Thompson, J. S. Vaagen, and M. V. Zhukov, Nucl. Phys. **A 632**, 383 (1998).

[88] S. Bacca, N. Barnea, and A. Schwenk, Phys. Rev. **C 86**, 034321 (2012).

[89] G. Hagen, D. J. Dean, M. Hjorth-Jensen, and T. Papenbrock, Phys. Lett. **B 656**, 169 (2007).

[90] M. Brodeur et al., Phys.Rev.Lett. **108**, 052504 (2012).

[91] K. Hagino, A. Vitturi, F. Pérez-Bernal and H. Sagawa, J. Phys. G: Nucl. Part. Phys. **38**, 015105 (2011).

[92] A. Vitturi and F. Pérez-Bernal, Nucl. Phys. **A 834**, 428c (2010).

[93] K. Heyde, *Basic ideas and concepts in nuclear physics, 3rd Ed.*, (IOP Publishing Ltd, Bristol, UK 2004).

[94] S. Aoyama, S. Mukai, K. Kato and K. Ikeda, Prog. Theor. Phys. **94**, 343 (1995).

[95] C. A. Bertulani and M. S. Hussein, Phys. Rev. **C 76**, 051602 (2007).

[96] K. Hagino and H. Sagawa, Phys. Rev. C **76**, 047302 (2007).

[97] Jagjit Singh, AIP Conf. Proc. **1681**, 020009 (2015).

[98] Jagjit Singh, L.Fortunato, to be published in Acta Physica Polonica B.

[99] Jagjit Singh, L.Fortunato, A.Vitturi and R.Chatterjee, to be submitted soon.

[100] A. de Shalit and I. Talmi, *Nuclear Shell Theory* (Academic Press,New York, 1963).

[101] J. Dobaczewski et al., Phys. Rev. **C 53**, 2809 (1996).

[102] G. F. Bertsch and H. Esbensen, Ann.Phys. **209**, 327-363 (1991).

[103] N. Austern, C. M. Vincent and J. P. Farrell Jr., Ann.Phys. **114**, 93-122 (1978).

[104] M. Kamimura, M. Yahiro, Y. Iseri, Y. Sakuragi, H. Kameyama and M. Kawai, Prog. Theor. Phys. Suppl. **89**, 1 (1986).

[105] N. Austern, Y. Iseri, M. Kamimura, M. Kawai, G. H. Rawitscher and M. Yahiro, Phys. Reports. **154**, 125 (1987).

[106] M. Yahiro, N. Nakano, Y. Iseri and M. Kamimura Prog. Theor. Phys. **67**, 1467 (1982).

[107] A. Csótó and G. M. Hale, Nuclear Physics **A 631**, 783 (1998).

[108] M. Yahiro and M. Kamimura, Prog. Theor. Phys. **65**, 2046 (1981); **65**, 2051 (1981).

[109] M. S. Golovkov, L. V. Grigorenko, A. S. Fomichev et al., Phys. Rev. **C 76**, 021605 (2007).

[110] R. A. D. Piyadasa, M. Kawai, M. Kamimura and M. Yahiro, Phys. Rev. **C 60**, 044611(1999).

[111] A. M. Moro, J. M. Arias, J. Gómez-Camacho, I. Martel, Pérez-Bernal, R. Crespo and F. Nunes, Phys. Rev. **C 65**, 011602 (2002).

[112] R. Y. Rasoanaivo and G. H. Rawitscher, Phy. Rev. **C 39**, 1709 (1989).

[113] T. Matsumoto, T. Kamizato, K. Ogata, Y. Iseri, E. Hiyama, M. Kamimura, and M. Yahiro, Phys. Rev. **C 68**, 064607 (2003).

[114] F. Pérez-Bernal, I. Martel, J. M. Arias, and J. Gómez-Camacho, Few-Body Syst. Suppl. **13**, 217 (2002).

[115] A. M. Moro, J. M. Arias, J. Gómez-Camacho and F. Pérez-Bernal, Phys. Rev. **C 80**, 054605 (2009).

[116] T. Matsumoto, E. Hiyama, M. Yahiro, K. Ogata, Y. Iseri, and M. Kamimura, Nucl. Phys. **A 738**, 471 (2004).

[117] M. Rodríguez-Gallardo, J. M. Arias, J. Gómez-Camacho, R. C. Johnson, A. M. Moro, I. J. Thompson, and J. A. Tostevin, Phys. Rev. **C 77**, 064609 (2008).

[118] TUNL, Nuclear Data Evaluation, `http://www.tunl.duke.edu/NuclData/General_Tables/5he.shtml`.

[119] D. R. Tilley, C. M. Cheves, J. L. Godwin, G. M. Hale, H. M. Hofmann, J. H. Kelley, G. Sheu, and H. R. Weller, Nucl. Phys. **A 708**, 3 (2002).

[120] Hiroshi Masui, Shigeyoshi Aoyama, Takayuki Myo, Kiyoshi Kat = o and Kiyomi Ikeda, Nucl. Phys. **A 673**, 207 (2000).

[121] M. T. Yamashita, T. Frederico and Lauro Tomio, Phys. Rev. **C 72**, 011601(R) (2005).

[122] T.Myo et al., Progress in Particle and Nuclear Physics **79**, 1-56 (2014).

[123] J. Kantele, Nucl. Instr. Meth. **A271** 625, (1988).

[124] J. Meyer, P. Quentin and M. Brack, Physics Letters **133B**, 279 (1983).

[125] S. Aoyama, S. Mukai, K. Kato and K. Ikeda, Prog. Theor. Phys. **116**, 1 (2006).

[126] P. Descouvemont, E. Pinilla, and D. Baye, Prog. Theor. Phys. Suppl. 196, 1 (2012).

[127] J. A. Lay, A. M. Moro, J. M. Arias, and J. Gómez-Camacho, Phys. Rev. **C 82**, 024605 (2010).